Available online at www.sciencedirect.com
SCIENCE DIRECT®
Finite Elements in Analysis and Design 39 (2003) 1191–1235
FINITE ELEMENTS IN ANALYSIS AND DESIGN
www.elsevier.com/locate/finel

A gradient model for finite strain elastoplasticity coupled with damage

P.M.A. Areias, J.M.A. César de Sá, C.A. Conceição António*

Instituto de Engenharia Mecânica (IDMEC), Faculdade de Engenharia da Universidade do Porto, Rua Dr. Roberto Frias s/n 4200-465 Porto, Portugal

Received 30 May 2001; accepted 7 January 2002

Abstract

This paper describes the formulation of an implicit gradient damage model for finite strain elastoplasticity problems including strain softening. The strain softening behavior is modeled through a variant of Lemaitre's damage evolution law. The resulting constitutive equations are intimately coupled with the finite element formulation, in contrast with standard local material models. A 3*D* finite element including enhanced strains is used with this material model and coupling peculiarities are fully described. The proposed formulation results in an element which possesses spatial position variables, nonlocal damage variables and also enhanced strain variables. Emphasis is put on the exact consistent linearization of the arising discretized equations.

A numerical set of examples comparing the results of local and the gradient formulations relative to the mesh size influence is presented and some examples comparing results from other authors are also presented, illustrating the capabilities of the present proposal.

1. Introduction

A standard implementation of constitutive equations which include strain softening behavior results, in general, unsatisfactory (see the analysis carried out in Ref. [1]). The reason for this is the observed dependency of the obtained results with mesh size and orientation, specially in the neighborhood of localized strain area [2,3]. This dependency can be explained by the change of type of the equilibrium equations [4,3]. A variety of discrete approaches has been applied as a remedy to attenuate this fact. For ductile fracture analyses, cohesive elements can be adopted as recently shown in Ref. [5]. The

* Corresponding author. Tel.: +351-22-508-1766; fax: +351-22-508-1445.
E-mail address: cantonio@fe.up.pt (C.A.C. António).

0168-874X/03/$ - see front matter © 2002 Elsevier B.V. All rights reserved.
PII: S0168-874X(02)00164-6

straightforward use of cohesive elements is, however limited to the cases where the fracture path is known.

For more general situations, a nonlocal or a gradient model can be adopted. Most of the work done concerning these models is, however, restricted to small strain situations. If this can be accepted in some materials and applications, the common ductile metal behavior presents finite plastic strains before and during the occurrence of instability and necking.

For finite strain situations, the work of Steinmann for hyper-elastic materials [6] and the work of Geers et al. for large strain plasticity [7,8] are relevant exceptions. Both these works, although in different contexts, use an implicit gradient model (see also Ref. [9] for a small strain brittle case and [10] for the small strain elastoplastic case).

The gradient models can be related to nonlocal models [11,12] which are known to be effective in attenuating the influence of mesh upon the results (Refs. [6,7] show the direct relation between the two approaches, including some needed simplifications).

Generally, gradient models are of simpler computer implementation than classic nonlocal models in the finite element context and also include the length scale information through a length scale parameter.

In the present work the adopted nonlocal variable is the damage scalar variable, and use is made of a version of the Lemaitre's damage model (described in Refs. [13,14]). The material length scale is controlled by a single parameter corresponding to the scale where strain localization occurs.

The finite element implementation of the proposed gradient constitutive law is carried out through a mixed enhanced formulation, resulting in the following set of nodal variables:

- nodal displacements;
- nodal damage variables;

and also internal (local) variables resulting from the adopted particular finite element technique:

- enhanced strain variables.

The proposed enhanced strain formulation is detailed for the fully three-dimensional case and consists of an evolution of the variationally consistent mixed plane-strain formulation proposed in Ref. [15].

2. General formulation

The extension of well established small-strain developments to include large strains, in particular large *plastic* strains, can be carried out through a variety of methodologies (see Refs. [16–24]). A comprehensive exposition of the classical ones is given in Ref. [25].

In this paper the authors are concerned with *isotropic* situations and with metal plasticity involving moderate elastic strains.

A finite elastoplasticity formulation based upon some key-features of the theory developed by Miehe [19,20] is adopted, but is here specialized for the damage coupling equations and with the inclusion of an implicit gradient formulation.

Recent developments [20,16] are supported by a decomposition that *circumvents* the explicit use of multiplicative decomposition of the deformation gradient and the so called stress-free intermediate

configuration, concepts that were exploited in other approaches [24,26,17]. For the isotropic case, the developments of Miehe [19,20,27] result in a formulation closely related to one of Simo [24] and both contrast with the relations derived by Brunig [16] where the material setting was chosen.

The following exposition, although reasonably standard for elastoplastic problems, has not, in the authors' knowledge, been applied for the developments involving gradient damage and elastoplastic coupling. The fundamental concepts are first outlined.

Let the tensors $\boldsymbol{g}$ and $\boldsymbol{G}$ denote the covariant metric tensors defined on the spatial and material configurations, respectively. Although the actual computer implementation is here carried out in orthonormal axes (which imply that, when represented in those axes, the metric tensors possess identity scalar component matrices), there are some nomenclature details revealed due to the introduction of these metric tensors [20,16,6].

The following set of *internal* variables, defined in the material setting, is presented:

- Right Cauchy–Green tensor, which can be introduced as the pull-back of the spatial metric tensor: $\boldsymbol{C} = \boldsymbol{F}^{\mathrm{T}}\boldsymbol{F} = \varphi^*(\boldsymbol{g})$, whose work conjugate field is the second Piola–Kirchhoff stress tensor, with the notation $\boldsymbol{S}$.
- Covariant plastic metric (on the material setting): $\boldsymbol{C}^P$ which possesses the initial condition $\boldsymbol{C}_0^P = \boldsymbol{G}$.

A comprehensive account of the pull-back and push-forward nomenclature is given in the book of Bonet and Wood [28].

The inclusion of the covariant plastic metric tensor is decisive to the description of the plastic evolution through the flow law. The tensor $\boldsymbol{C}^P$ is a symmetric, positive definite tensor [19], which restricts the flow law to be six dimensional as in the small strain case (without the consideration of the constitutive isotropy).

The deformation gradient, previously denoted as $\boldsymbol{F}$, is a two point tensor (mixed Eulerian–Lagrangian), which may be decomposed according to the following notation (see also [29]):

$$\boldsymbol{F} = \frac{\partial \varphi^a}{\partial X^A}\boldsymbol{e}_a \otimes \boldsymbol{E}^A = F^a_{\ A}\boldsymbol{e}_a \otimes \boldsymbol{E}^A, \tag{1}$$

where the function $\boldsymbol{x} = \varphi(\boldsymbol{X})$ is the deformation map.

The vectors $\boldsymbol{E}^A$ and $\boldsymbol{e}_a$ in (1) form vector bases of the material configuration and spatial configuration, respectively. The dual vectors, $\boldsymbol{E}_A$ and $\boldsymbol{e}^a$ are defined according to the relations $\boldsymbol{E}^A \cdot \boldsymbol{E}_B = \delta^A_B$ and $\boldsymbol{e}^a \cdot \boldsymbol{e}_b = \delta^a_b$.

A fundamental concept used by some authors [19,16] is the so-called *mixed variant elastic strain measure* which can be presented as the following tensor product:

$$\boldsymbol{C}^e = \boldsymbol{C}\boldsymbol{C}^{p-1}. \tag{2}$$

It is clear that $\boldsymbol{C}$ itself is a mixed variant *contravariant–covariant* tensor (see Ref. [29]).

The decomposition (2) circumvents the otherwise necessary concept of *rotation* related to the stress-free intermediate local configuration (adopted in Refs. [26,24,30]).

A spatial tensor which can be defined through the (material) covariant plastic metric is the so-called elastic left Cauchy–Green tensor, which may be written according to

$$\boldsymbol{b}^e = \boldsymbol{F}\boldsymbol{C}^{p-1}\boldsymbol{F}^{\mathrm{T}}. \tag{3}$$

This definition (3) is particularly convenient when writing the plastic flow law in the spatial configuration, as it will become apparent. It is important to state that relation (3) represents a definition, and it is not a consequence of the elastic deformation gradient (which is not defined in the present work), as it is the case with formulations based upon the stress-free intermediate configuration.

A locally defined stored energy isotropic function is now introduced, and it is assumed to depend on the right Cauchy–Green strain tensor, the covariant plastic metric, a scalar internal variable related to the plastic irreversibility and hardening identified by the letter A, and a scalar damage variable identified by the letter D:

$$\psi(\boldsymbol{C}, \boldsymbol{C}^p, A, D). \tag{4}$$

Expression (4) implies that the degradation due to damage is an isotropic effect and also that the internal irreversibility is *also* an isotropic effect, and therefore kinematic hardening is precluded.

In terms of damage, it has been concluded (in Ref. [14]) that this type of model is suitable for proportional loading situations.

The time derivative of the stored energy function (4) takes the following form:

$$\dot{\psi} = \partial_{\boldsymbol{C}}\psi\colon \dot{\boldsymbol{C}} + \partial_{\boldsymbol{C}^p}\colon \dot{\boldsymbol{C}}^p + \partial_A\psi\dot{A} + \partial_D\psi\dot{D}. \tag{5}$$

The evolution laws for the proposed thermodynamic variables are derived to satisfy *ab initio* the second law of thermodynamics, which is here presented in the local form of the Clausius–Planck inequality, ignoring thermal effects:

$$\mathscr{D}_{\text{int}} = \tfrac{1}{2}\boldsymbol{S} : \dot{\boldsymbol{C}} - \dot{\psi} \geqslant 0, \tag{6}$$

where the equality case corresponds to a conservative or reversible process.

Inserting Eq. (5) into the inequality (6), it is possible to rewrite (6) according to the following notation:

$$\mathscr{D}_{\text{int}} = \left(\tfrac{1}{2}\boldsymbol{S} - \partial_{\boldsymbol{C}}\psi\right) : \dot{\boldsymbol{C}} - \partial_A\psi\dot{A} - \partial_{\boldsymbol{C}^p}\psi\colon \dot{\boldsymbol{C}}^p - \partial_D\psi\dot{D} \geqslant 0. \tag{7}$$

Furthermore, the following constitutive relation is assumed for the second Piola–Kirchhoff stress tensor $\boldsymbol{S}$:

$$\boldsymbol{S} = 2\partial_{\boldsymbol{C}}\psi \tag{8}$$

which is specially convenient, as it implies that, if the relations $\dot{A} = \dot{D} = 0$ and also $\dot{\boldsymbol{C}}^p = \boldsymbol{0}$ are satisfied, then the process is conservative, because $\mathscr{D}_{\text{int}} = 0$ for an arbitrary $\dot{\boldsymbol{C}}$. As the term $\dot{\boldsymbol{C}}$ is a direct consequence of the deformation history, in the case of absence of evolution for A and D, then (8) ensures that the process is conservative for *any* deformation history.

The conjugate variables (also usually denominated thermodynamic forces [19]) of the proposed thermodynamic variables A, D and $\boldsymbol{C}^p$ are denoted B, which is the *internal force*, Y, which is designated the *strain energy release rate* and $\boldsymbol{S}^p$ which is designated the *plastic force*, respectively.

Concisely, these thermodynamic forces are given by

$$\boldsymbol{S} = 2\partial_{\boldsymbol{C}}\psi\,, \tag{9a}$$

$$\boldsymbol{S}^p = \partial_{\boldsymbol{C}^p}\psi\,, \tag{9b}$$

$$B = \partial_A \psi\,, \tag{9c}$$

$$Y = -\partial_D \psi\,. \tag{9d}$$

The function $\mathscr{D}_{\text{int}}$ in (7) may be interpreted as an inner product [19].

Other authors use a distinct sign convention for definitions (9), but this fact should not cause apprehension at this point, as the actual relations depend exclusively on the particular form adopted for the stored energy function, ψ, as it will become apparent.

Using relations (9), the local form of the Clausius–Planck inequality (7), without the contribution of the thermal effects, takes the following aspect:

$$\mathscr{D}_{\text{int}} = -\boldsymbol{S}^p\colon \dot{\boldsymbol{C}}^p - B\dot{A} + Y\dot{D} \geqslant 0. \tag{10}$$

Before a full characterization of the remaining constitutive equations, a yield function is introduced. The yield function is assumed to depend upon the plastic force $\boldsymbol{S}^p$, the internal force B, the damage variable D and the covariant plastic metric $\boldsymbol{C}^p$, in agreement with the following expression:

$$\phi(\boldsymbol{S}^p, B, D, \boldsymbol{C}^p). \tag{11}$$

With the yield function presented according to (11), it is possible to establish an "elastic domain", identified by E, as the next set of ordered pairs $(\boldsymbol{S}^p, B)$:

$$E = \{(\boldsymbol{S}^p, B) \in \Re^6 \times \Re \,|\, \phi(\boldsymbol{S}^p, B, D, \boldsymbol{C}^p) \leqslant 0\}. \tag{12}$$

For the associative case [20,24], the yield function is simultaneously a dissipative potential, and the evolution equations for the thermodynamic variables are frequently derived making use of the principle of maximum plastic dissipation (see also Ref. [18] for an account on the derivation of flow laws). The flow law in the present paper is nonassociative, and therefore an additional scalar function must be introduced, usually denominated *potential of dissipation* which is an isotropic and convex function of its arguments:

$$\mathscr{F}(\boldsymbol{S}^p, B, Y, \boldsymbol{C}^p, D, A). \tag{13}$$

Having defined the potential of dissipation (13), the evolution laws for the internal variables are subsequently *postulated* as follows:

$$\dot{\boldsymbol{C}}^p = \dot{\alpha}\partial_{\boldsymbol{S}^p}\mathscr{F}, \tag{14a}$$

$$\dot{A} = -\dot{\alpha}\partial_B \mathscr{F}, \tag{14b}$$

$$\dot{D} = \dot{\alpha}\partial_Y \mathscr{F}, \tag{14c}$$

where $\dot{\alpha}$ in (14) is the plastic parameter. For associative evolution laws the term $\dot{\alpha}$ is commonly denominated *plastic multiplier* as, in that case, it corresponds to a Lagrange multiplier [19,25,18]. With some abuse of notation, $\dot{\alpha}$ may be also denominated *plastic multiplier* in the present nonassociative situation.

Making use of the definition of the plastic force in Eq. (9b), it is possible to calculated it as

$$\boldsymbol{S}^p = \tfrac{1}{2}\boldsymbol{C}^{p-1}\boldsymbol{C}\boldsymbol{S}. \tag{15}$$

The yield function (11) and the potential of dissipation (13) are taken as functions of the mixed-variant stress [19] $\boldsymbol{C}\boldsymbol{S}$ and adopt the following forms:

$$\phi(\boldsymbol{C}\boldsymbol{S}, B, D) \tag{16a}$$

and

$$\mathscr{F}(\boldsymbol{C}\boldsymbol{S}, B, Y, D, A), \tag{16b}$$

respectively.

The motivation for the use of the mixed-variant stress $\boldsymbol{C}\boldsymbol{S}$ in relations (16) is related to the derived form (15) and the purpose of avoiding the dependence of the yield function and the potential of dissipation upon the covariant plastic metric.

After some algebraic operations, the flow law presented in (14a) can be restated in agreement with the following form:

$$\dot{\boldsymbol{C}}^p = 2\dot{\alpha}\boldsymbol{C}^p\frac{\partial\mathscr{F}}{\partial\boldsymbol{C}\boldsymbol{S}} = 2\dot{\alpha}\boldsymbol{C}^{e-1}\frac{\partial\mathscr{F}}{\partial\boldsymbol{S}}. \tag{17}$$

Inverting the previous form of the flow law (17), the following equation emerges:

$$\dot{\boldsymbol{C}}^{p-1} = -2\dot{\alpha}\boldsymbol{C}^p\frac{\partial\mathscr{F}}{\partial\boldsymbol{S}}\boldsymbol{C}^{p-1} \tag{18}$$

which is rigorously the same flow law derived by Simo [26,24] in the context of the multiplicative decomposition concept.

Eq. (18) can be written in the spatial setting as

$$\boldsymbol{F}\dot{\boldsymbol{C}}^{p-1}\boldsymbol{F}^{\mathrm{T}} = -2\dot{\alpha}\boldsymbol{F}^{-\mathrm{T}}\frac{\partial\mathscr{F}}{\partial\boldsymbol{S}}\boldsymbol{C}^e\boldsymbol{F}^{-1} = -2\dot{\alpha}\boldsymbol{F}^{-\mathrm{T}}\frac{\partial\mathscr{F}}{\partial\boldsymbol{S}}\boldsymbol{F}^{-1}\boldsymbol{F}^{-\mathrm{T}}\boldsymbol{C}^e\boldsymbol{F}^{\mathrm{T}}. \tag{19}$$

Therefore, making use of definition (3) and introducing the Kirchhoff stress tensor as the push-forward of the second Piola–Kirchhoff stress tensor,

$$\boldsymbol{\tau} = \boldsymbol{F}\boldsymbol{S}\boldsymbol{F}^{\mathrm{T}} \tag{20}$$

it is possible to write the following relation:

$$\boldsymbol{F}\dot{\boldsymbol{C}}^{p-1}\boldsymbol{F}^{\mathrm{T}} = -2\dot{\alpha}\frac{\partial\mathscr{F}}{\partial\boldsymbol{\tau}}\boldsymbol{b}^e \tag{21}$$

in which was made of the relation $\partial\mathscr{F}/\partial\boldsymbol{S} = \boldsymbol{F}^{\mathrm{T}}(\partial\mathscr{F}/\partial\boldsymbol{\tau})\boldsymbol{F}$.

If the Lie derivative of $\boldsymbol{b}^e$ relative to the spatial velocity is introduced [24,19,25], such as $\mathscr{L}_v\boldsymbol{b}^e = \boldsymbol{F}\partial_t(\boldsymbol{F}^{-\mathrm{T}}\boldsymbol{b}^e\boldsymbol{F}^{-1})\boldsymbol{F}^{\mathrm{T}}$, the flow law in the spatial setting takes the same format as in Simo [24] or Ibrahimbegovic and Gharzeddine [17] within the framework of the multiplicative decomposition of the deformation gradient:

$$\mathscr{L}_v\boldsymbol{b}^e = -2\dot{\alpha}\frac{\partial\mathscr{F}}{\partial\boldsymbol{\tau}}\boldsymbol{b}^e. \tag{22}$$

The purpose of this short exposition was to clarify and detail the steps that lead to (22), which may seem an odd equation when compared with the small-strain plastic flow law (exposed, for example in Ref. [18]). Additionally, the presence of the damage variable and its conjugate appears as a simple extension of the coupled small strain case discussed in classical Refs. [13,14].

The second Piola–Kirchhoff stress tensor $\boldsymbol{S}$ introduced in Eq. (8), can also be evaluated using derivatives relative to $\boldsymbol{C}^e$ or $\boldsymbol{C}^p$, instead of $\boldsymbol{C}$:

$$\boldsymbol{S} = 2\boldsymbol{C}^{e-1}\partial_{\boldsymbol{C}^p}\psi = 2\boldsymbol{C}^{-1}\boldsymbol{C}^p\partial_{\boldsymbol{C}^p}\psi\,. \tag{23}$$

A similar relation for the Kirchhoff stress tensor can be derived in the spatial setting through relation (23) and Eq. (20) which relates the material and spatial stress tensors.

After some algebraic operations, it is possible to obtain the following constitutive law for the Kirchhoff stress tensor:

$$\boldsymbol{\tau} = 2\partial_{\boldsymbol{b}^e}\psi\boldsymbol{b}^e. \tag{24}$$

Eq. (24) is worthy of the following observation: if the tensor[1] $\boldsymbol{C}^p$, which describes the plastic deformation state, is known in a particular point (and therefore $\boldsymbol{b}^e$ is also known at that point through the deformation gradient (3)), the Kirchhoff stress tensor is determined by Eq. (24). As a consequence, the use of the so-called incremental objective algorithms (see, for instance, the Ref. [31]) is not required, as the stress tensor is obtained directly by relation (24).

Additionally, the stored energy function can then take the following decomposed form (in the spatial setting):

$$\psi(\boldsymbol{b}^e, A, D) = (1-D)\psi^e(\boldsymbol{b}^e) + \psi^p(A), \tag{25}$$

where ψ^e is a function of the elastic left Cauchy–Green tensor exclusively, and ψ^p is the part related to the plastic hardening governed by the internal variable A. This decomposed form is useful in the extension of the small strain concepts of damage mechanics (see Refs. [14,32]) to the finite strain range.

The potential of dissipation is also assumed to be decomposable as a sum of the yield function and a damage-related potential of dissipation, $\mathscr{F}_{\mathscr{D}}$, in agreement with previous notations:

$$\mathscr{F}(\boldsymbol{\tau}, B, Y, D, A) = \phi(\boldsymbol{\tau}, B, D) + \mathscr{F}_{\mathscr{D}}(Y, D, A). \tag{26}$$

The particular form (26) allows the partial decoupling between the damage effects and the irreversibility effects due to plastic evolution. The coupling that remains is due to the presence of the damage variable, D in the two terms of Eq. (26).

Making use of the decomposed forms of the stored energy function (25) and the potential of dissipation in form (26), the set of constitutive equations in the spatial setting is briefly summarized in Table 1. This type of convenient decompositions (25) and (26) has been adopted both in the small strain case [13,14] and finite strain case [33,34].

[1] Or, in more accurate terms, the tensor representation $\boldsymbol{C}^p$, as a tensor is a multilinear functional (see [29]).

Table 1
Set of evolution laws for the thermodynamic variables and definition of conjugate variables

Plastic flow law	$\mapsto$	$\mathscr{L}_v \boldsymbol{b}^e = -2\dot{\alpha}\dfrac{\partial \phi}{\partial \boldsymbol{\tau}}\boldsymbol{b}^e$
Damage evolution law	$\mapsto$	$\dot{D} = \dot{\alpha}\dfrac{\partial \mathscr{F}_{\mathscr{D}}}{\partial Y}$
Internal variable evolution law	$\mapsto$	$\dot{A} = -\dot{\alpha}\dfrac{\partial \phi}{\partial B}$
Loading/unloading conditions	$\mapsto$	$\dot{\alpha} \geqslant 0;\ \phi \leqslant 0;\ \dot{\alpha}\phi = 0$
Kirchhoff stress	$\mapsto$	$\boldsymbol{\tau} = 2(1-D)\partial_{\boldsymbol{b}^e}\psi^e \boldsymbol{b}^e$
Strain energy release rate	$\mapsto$	$Y = -\partial_D \psi = \psi^e$
Internal force	$\mapsto$	$B = \partial_A \psi^p$

Assuming orthogonal axes, the elastic left Cauchy–Green tensor (3), may be spectrally decomposed according to the expression:

$$\boldsymbol{b}^e = \lambda_k^2 \boldsymbol{n}_k \otimes \boldsymbol{n}_k \text{ summation implied}, \tag{27}$$

where $\boldsymbol{n}_k$ represent the (unitary) principal directions and λ_k^2 represent the principal values of $\boldsymbol{b}^e$.

The particular form (27) is possible as the tensor $\boldsymbol{b}^e$ is symmetric and positive-definite.

The elastic part of the stored energy isotropic function, ψ^e, is assumed to depend upon the tensor $\boldsymbol{b}^e$ according to the following relation:

$$\psi^e = \psi^e(\varepsilon_1, \varepsilon_2, \varepsilon_3), \tag{28}$$

where ε_k denote the elastic principal strains, which can be written as

$$\varepsilon_k = \ln[\lambda_k], \tag{29}$$

where the terms λ_k are the *positive* square roots of λ_k^2.

The elastic principal strains in (29) are components of the elastic spatial Hencky strain tensor.

Making use of the relation $\boldsymbol{n}_i \cdot \boldsymbol{b}^e \boldsymbol{n}_i = \lambda_i^2$, the Kirchhoff stress tensor may be written as well in principal directions:

$$\boldsymbol{\tau} = \tau_k \boldsymbol{n}_k \otimes \boldsymbol{n}_k = \Omega \frac{\partial \psi^e}{\partial \varepsilon_k} \boldsymbol{n}_k \otimes \boldsymbol{n}_k \tag{30}$$

with $\Omega = 1 - D$.

With the Kirchhoff stress tensor spectrally decomposed in agreement with Eq. (30), the spatial *elasticity* tensor for the Truesdell rate, which is here denoted as $\boldsymbol{C}_T$, can be calculated as (see also Refs. [28,27]):

$$\boldsymbol{C}_T = \sum_{i=1}^{3}\sum_{j=1}^{3} \frac{\partial \tau_i}{\partial \varepsilon_j} \boldsymbol{n}_i \otimes \boldsymbol{n}_j \otimes \boldsymbol{n}_i \otimes \boldsymbol{n}_j - 2\sum_{i=1}^{3} \tau_i \boldsymbol{n}_i \otimes \boldsymbol{n}_i \otimes \boldsymbol{n}_i \otimes \boldsymbol{n}_i \tag{31}$$

$$+ \sum_{i=1}^{3}\sum_{j\neq i=1}^{3} r_{ij} \boldsymbol{n}_i \otimes \boldsymbol{n}_j \otimes (\boldsymbol{n}_i \otimes \boldsymbol{n}_j + \boldsymbol{n}_j \otimes \boldsymbol{n}_i), \tag{32}$$

where

$$r_{ij} = \begin{cases} \frac{\lambda_j^2\tau_i - \lambda_i^2\tau_j}{\lambda_i^2 - \lambda_j^2} & : \lambda_i \neq \lambda_j, \\ \frac{1}{2}\left(\frac{\partial\tau_j}{\partial\varepsilon_j} - \frac{\partial\tau_i}{\partial\varepsilon_i} - 2\tau_j\right) & : \lambda_i = \lambda_j. \end{cases} \tag{33}$$

The only terms in Eq. (32) that depend on the particular constitutive law adopted is the term $\partial\tau_i/\partial\varepsilon_j$, and, in the second branch of (33), the terms $\partial\tau_j/\partial\varepsilon_j$ and $\partial\tau_i/\partial\varepsilon_i$. The coefficient matrix of $\partial\tau_i/\partial\varepsilon_j$ is here denoted $\boldsymbol{C}^{\varepsilon}$.

The isotropic yield function may be written as a function of the principal Kirchhoff stresses (see first term of definition (26)):

$$\phi = \phi(\tau_1, \tau_2, \tau_3, B, D) \tag{34}$$

and the flow law in the spatial configuration (22) takes the following form:

$$\mathscr{L}_v \boldsymbol{b}^e = -2\dot{\alpha} \sum_{i=1}^{3} \frac{\partial\phi}{\partial\tau_i} \lambda_i^2 \boldsymbol{n}_i \otimes \boldsymbol{n}_i. \tag{35}$$

Furthermore, the principal stresses τ_i can be grouped in an one-dimensional array as

$$\boldsymbol{\sigma} = \begin{Bmatrix} \tau_1 \\ \tau_2 \\ \tau_3 \end{Bmatrix}. \tag{36}$$

In an analogous form, the principal elastic strains can also be grouped in an one-dimensional array as

$$\boldsymbol{\varepsilon} = \begin{Bmatrix} \varepsilon_1 \\ \varepsilon_2 \\ \varepsilon_3 \end{Bmatrix}. \tag{37}$$

The notation $\boldsymbol{\sigma}$ and $\boldsymbol{\varepsilon}$ is intentional and reflects the existence of an analogy with the small strain case in principal directions, a fact exploited by Simo [24].

3. Constitutive equations for elastoplasticity including isotropic damage

Having exposed the participating variables and functions, a further step is needed toward the complete description of the material model. The specific functions are subsequently presented, both for a local and a new gradient approach, which can be considered particular cases of the exposure in Section 2.

A summary of the relevant features in the damage–deformation coupling is next briefly presented.

In the plastic deformation of metals, the ductile damage process occurs simultaneously with large plastic deformations, and the kinetic law of damage should reflect the evolution of the ductile damage

process: nucleation, growth and coalescence of micro-voids, as fully discussed in Refs. [14,35,36] (in the nucleation phase it is assumed that there is a null damage evolution).

In short, the nucleation process is due to the presence of inclusions and second phase particles and occurs when there is an interface decohesion or when particles crack. Following this phase, the growth of the nucleated voids is controlled by plastic strain and hydrostatic pressure, and the final coalescence process is due to plastic localization as the voids get larger and interact between each other (see a detailed description in Ref. [35]). As the nucleation of (micro)voids is known to have no effect on the mechanical properties, the threshold for damage evolution should reflect this fact [14]. This threshold is related to the start of the necking phenomenon in the uniaxial tension test.

The ductile damage evolution is assumed to occur when the internal variable A, related to the plastic deformation (irreversibility), exceeds a certain threshold value, denoted here as A_D. In fact, this threshold can depend upon the loading, the fatigue limit and the ultimate stress [14]. Notwithstanding, in this work, for simplicity reasons, it is assumed that the threshold for damage evolution is a material property, which can be extracted from the uniaxial tension test.

The particular form for the damage part of the potential of dissipation introduced in Eq. (26) is the same proposed by Lemaitre [13,14] with an exponent of 2:

$$\mathscr{F}_{\mathscr{D}} = \frac{Y^2}{2S_0(1-D)} H(A - A_D), \tag{38}$$

where $H(x)$ denotes the Heaviside function of a generic real argument x, and S_0 is a material property representing the energy strength of damage, which is tabulated for some materials in Ref. [14].

The damage evolution law follows in a straightforward manner (see Eq. (14c)):

$$\dot{D} = \dot{\alpha} H(A - A_D) \frac{Y}{S_0 \Omega}. \tag{39}$$

A extension of (39) is included to impose the critical damage value: if $D \geqslant D_c$ then $D = D_u$, where D_c represents the critical damage and D_u is the residual damage value, with a value close to 1.

The yield function for the von-Mises case coupled with damage can be expressed as

$$\phi = \sqrt{\frac{3}{2}} \frac{\|\boldsymbol{s}\|}{\Omega} - B(A), \tag{40}$$

where the internal force B is a known function of the internal variable A and $\boldsymbol{s}$ is the deviatoric part of the stress vector in principal directions, $\boldsymbol{\sigma}$, defined in (36).

According to the introduced notation, the norm $\|\boldsymbol{s}\|$ in (40) can be calculated as $\|\boldsymbol{s}\| = \sqrt{\boldsymbol{s} \cdot \boldsymbol{s}}$ where

$$\boldsymbol{s} = \boldsymbol{\sigma} - \tfrac{1}{3}(\tau_1 + \tau_2 + \tau_3) \begin{Bmatrix} 1 \\ 1 \\ 1 \end{Bmatrix}.$$

The pressure field (*using the small strain analogy*) can be calculated[2] as $\frac{1}{3}(\tau_1 + \tau_2 + \tau_3)$.

[2] In fact this is an approximation, as Kirchhoff stresses are adopted, not Cauchy stresses.

As a direct consequence of form (40), it is possible to recognize the following equality:

$$\dot{\alpha} = \dot{A}. \tag{41}$$

The spatial flow law in principal directions (35) may be further detailed with the help of (40) and the application of the chain rule:

$$\mathscr{L}_v \boldsymbol{b}^e = -\sum_{i=1}^{3} 2\dot{\alpha}\, \frac{\partial \phi}{\partial \|\boldsymbol{s}\|}\, \lambda_i^2 v_i \boldsymbol{n}_i \otimes \boldsymbol{n}_i, \tag{42}$$

where the vector $\boldsymbol{v}$ whose scalar components are v_i in (42), is defined according to

$$\boldsymbol{v} = \frac{\partial \|\boldsymbol{s}\|}{\partial \boldsymbol{s}} = \frac{\boldsymbol{s}}{\|\boldsymbol{s}\|} \tag{43}$$

and it is denominated *flow vector*.

Additionally, $\partial\phi/\partial\|\boldsymbol{s}\| = (1/\Omega)\sqrt{3/2}$ and therefore:

$$\mathscr{L}_v \boldsymbol{b}^e = -\sum_{i=1}^{3} 2\dot{\alpha} \sqrt{\frac{3}{2}}\, \lambda_i^2\, \frac{v_i}{\Omega}\, \boldsymbol{n}_i \otimes \boldsymbol{n}_i. \tag{44}$$

If the effective plastic strain rate is introduced as

$$\dot{\varepsilon}_p = \frac{\dot{\alpha}}{\Omega} \tag{45}$$

then Eq. (44) can be re-written in a more standard way (for the small strain case, consult Ref. [14] where extensive use was made of the *effective* plastic strain rate):

$$\mathscr{L}_v \boldsymbol{b}^e = -\sum_{i=1}^{3} 2\dot{\varepsilon}_p \sqrt{\frac{3}{2}}\, \lambda_i^2 v_i \boldsymbol{n}_i \otimes \boldsymbol{n}_i. \tag{46}$$

It remains to detail the particular forms for the scalar functions ψ^e and ψ^p, which are part of the stored energy function as assumed in relation (25). The form adopted in principal directions for the elastic stored energy function is (see Ref. [24] for a similar case, but without the presence of the damage variable):

$$\psi^e = \frac{9\kappa}{2}\,\theta^2 + \frac{3}{2}\mu(e_1^2 + e_2^2 + e_3^2), \tag{47}$$

where $\theta = \frac{1}{3}(\varepsilon_1+\varepsilon_2+\varepsilon_3)$ denotes the dilatation field and $e_i = \varepsilon_i - \theta$ denote the distortional components of the principal elastic strains. The symbols μ and κ represent the shear modulus and the bulk modulus, respectively.

The particular form (47), besides its analytical convenience, is particularly suitable for representing metal plasticity, as noted by Brunig [16] and Simo [24].

The principal stresses, as presented in Eq. (36) can therefore be written according to the following relations:

$$\tau_i = \Omega(2\mu e_i + 3\kappa\theta). \tag{48}$$

The compact elastic law (48) is possible due to the representation in principal axes.

The analytical expression for the function ψ^p, which allows the identification of the internal force, B, takes the following form, corresponding to a saturation model, as proposed in Refs. [24,30,21]:

$$\psi^p = \sigma_Y \alpha + (\sigma_\infty - \sigma_Y)\left(\alpha + \frac{1}{\delta}\mathrm{e}^{-\delta\alpha}\right) + \frac{1}{2}H\alpha^2, \tag{49}$$

where σ_Y, σ_∞, δ and H are material properties, which may be approximately evaluated through a uniaxial tension test (a least square methodology can be adopted in the evaluation of these material properties). An important aspect in relation (49) is that the term α is used and not ε_p so that α must be adopted in the final set of coupled equations, as it will become clear.

The functional dependence of the internal force, B in terms of the internal variable $\alpha = A$ follows directly from Eq. (49) and relation (9c):

$$B = \sigma_Y + (\sigma_\infty - \sigma_Y)(1 - \mathrm{e}^{-\delta\alpha}) + H\alpha. \tag{50}$$

An important and useful concept in the damage mechanics literature is the one related to the *effective stresses* [13,14], in opposition to the *homogenized stresses*, which were represented (in principal directions) by the array $\boldsymbol{\sigma}$ in Eq. (51). Using a one-dimensional analogy, the *effective stresses* in a given cross section may be understood as the stresses present in the remaining resisting deformed area, here denoted as S, whereas the homogenized stresses can be thought as the average stresses in the total deformed area, S/Ω (this physical interpretation is introduced in Ref. [13]).

As a convenience, the effective stresses are here distinguished with a tilde,

$$\tilde{\boldsymbol{\sigma}} = \frac{\boldsymbol{\sigma}}{\Omega}. \tag{51}$$

According to this notation, the deviatoric effective Kirchhoff stress can be denoted as $\tilde{\boldsymbol{s}}$ and the effective pressure can be denoted $\tilde{p}$. It is noticeable that relation (51) is written in principal directions.

Using this concept, the elastic stored energy function ψ^e, which also represents the strain energy release rate, as shown in Table 1, can be re-written as

$$\psi^e = Y = \frac{\|\tilde{\boldsymbol{s}}\|^2}{4\mu} + \frac{\tilde{p}^2}{2\kappa}. \tag{52}$$

A small strain $1D$ representation of the damage evolution law and the homogenized stress as a function of the total strain including the identification of some representative points is presented in Fig. 1.

The curves represented in Fig. 1 are presented for the case of absence of hardening, and for the following values: $E = 70 \times 10^9$, $\sigma_Y = 200 \times 10^6$, $S_0 = 1 \times 10^6$, $\alpha_D = 0.2$, $D_c = 0.8$, $D_u = 0.99$ and, of course, $\varepsilon_{pD} = \alpha_D$. No hardening has been included.

Although several authors have numerically implemented the set of equations discussed so far, within the so-called *local* approach (as opposed to *nonlocal* approaches), both in small strain [32,37,38] and finite strain [33,34] situations, this type of approach conveys a difficulty: For softening materials, the straightforward finite element implementation of the formulation discussed so far leads to results that are not independent of the adopted mesh. This dependency of the mesh manifests itself both relatively to the mesh size and to the mesh orientation. As localization of deformations occurs in very small areas, which are usually much smaller than the typical element size, this mesh size imposes the size of the numerically obtained localization areas. Also, the mesh direction has

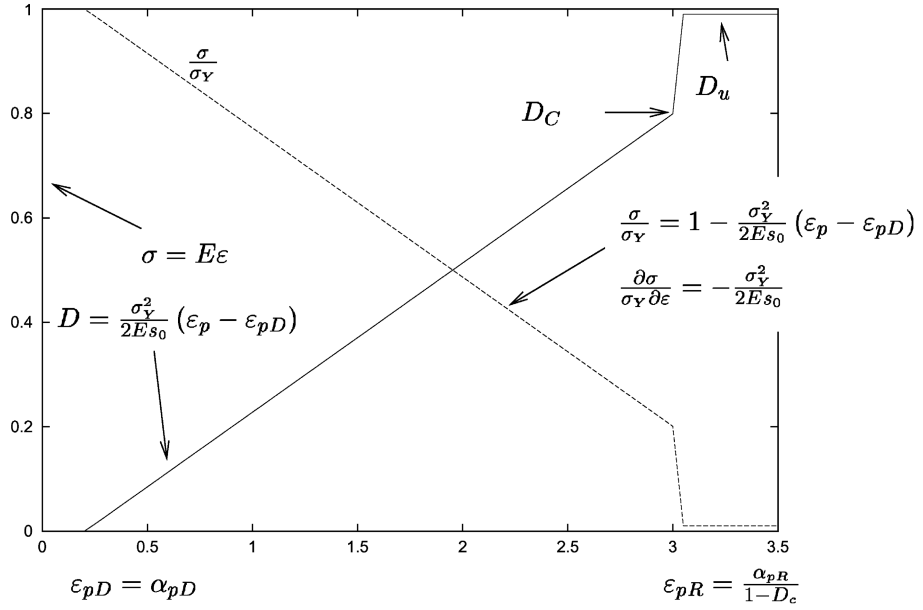

Fig. 1. The representation of the uniaxial behavior of damage evolution and homogenized stress.

an influence on the direction of the localized zones [39]. The reason for this is the local change on the type of the equilibrium equations which allow the discontinuity of strain. Further discussion of diagnostic and remedies for this behavior have been addressed in Refs. [9,2,10,40,12,8,1,41], for example.

Typical approaches to attenuate the mesh dependency behavior are: purely nonlocal models [11,41,12], explicit gradient models [4,42], implicit gradient models [1,8,7,2], artificial rate dependency, embedded discontinuity models [43], micro polar continua [44], and others (see [44,1] for more details). The procedure adopted in this paper is an implicit gradient method, which allows an implementation in a pre-existent finite element code (a Fortran 90 code created by the first author and called *SIMPLAS*).

Although numerous (see the references above) works have been published describing successful formulations of gradient plasticity and damage for small strain problems, few authors have addressed the finite strain situation.

Geers et al. [7,8] describe a large strain gradient-enhanced plasticity theory, where the nonlocal variable is the effective plastic strain and Steinmann [6] adopted a gradient formulation for elastic problems including damage.

An implicit gradient formulation is here applied to the derivations discussed in Section 2, but using a nonlocal damage variable. Although an important point in the finite strain implementations of gradient models is whether a material or spatial (or mixed [6]) average should be carried out (see the discussions in Refs. [6,7]), a material nonlocality is adopted in this paper, as it is favored by Steinmann [6] for elastic problems, both from the implementation and the results viewpoints.

The damage evolution law, as it was presented in Eq. (39), can now be considered valid for the *local* variable D, and the nonlocal damage variable is now presented as $\bar{D}$.

The effective stress and the homogenized stress in principal directions (51), for the gradient model, can be related according to

$$\boldsymbol{\sigma} = (1-\bar{D})\tilde{\boldsymbol{\sigma}}, \tag{53}$$

where use was made of the newly introduced nonlocal damage variable, $\bar{D}$. Therefore, the equilibrium equations are written using a *nonconstitutive* damage variable, $\bar{D}$. This variable is implicitly [3] related to the constitutive damage variable, D.

In an analogous form, the flow law for the gradient model can be written modifying (55) as follows:

$$\mathscr{L}_v \boldsymbol{b}^e = -\sum_{i=1}^{3} 2\dot{\alpha}\sqrt{\frac{3}{2}}\lambda_i^2 \frac{v_i}{\bar{\Omega}} \boldsymbol{n}_i \otimes \boldsymbol{n}_i, \tag{54}$$

where $\bar{\Omega} = 1-\bar{D}$.

The relation between the local damage field D, and the nonlocal damage field $\bar{D}$ can be written as (see also Ref. [6]):

$$\bar{D} - c_0 \nabla_0^2 \bar{D} : \boldsymbol{I} = D, \tag{55}$$

where c_0 is an area parameter also called *gradient* parameter and $\nabla_0^2\bar{D}$ is the material Hessian of the nonlocal damage, $\nabla_0^2\bar{D} : \boldsymbol{I}$ represents the material Laplacian.

The c_0 parameter in (55) can be calculated as the square of a length scale l_0 as $c_0 = l_0^2$.

The differential equation for $\bar{D}$ in (55) can be derived from a truly nonlocal integral form, as exposed in Ref. [6] for the stored energy case.

Eq. (55) has an analogous form to the one adopted in Ref. [7] for the plastic multiplier in the finite strain case and in Ref. [9] for the small strain case. Eq. (55) is a modified Helmholtz equation [2]. Another important aspect for the solution of this differential equation is the boundary conditions for $\bar{D}$ and $\nabla_0\bar{D}$. Although this aspect is not fully clarified and deserves much further study, we here follow the standard procedure of adopting homogeneous boundary condition for $\nabla_0\bar{D}$ in the boundary normal (in agreement with Refs. [6,9,2]) and $\bar{D}$ is left an unknown in the boundaries.

An integration of (55) for $\bar{D}$ is possible for unidimensional problems and known D. A study of the influence of c_0 in the relation between the two fields $\bar{D}$ and D is carried out for a known D. For constant D, the relation between $\bar{D}$ and D can be expressed as (if x is the only participating coordinate):

$$\bar{D} = \tfrac{1}{2}(c_1 + c_2 - D)\mathrm{e}^{x/\sqrt{c_0}} + \tfrac{1}{2}(c_1 - c_2 - D)\mathrm{e}^{-x/\sqrt{c_0}} + D, \tag{56}$$

where c_1 and c_2 are integration constants. It is clear that the important parameter in the relation between $\bar{D}$ and D as given by solution (56) is the square root of the area parameter, i.e. the length scale parameter $l_0 = \sqrt{c_0}$.

For the analytical study a uniaxial specimen with infinite length is analysed, with D null except in a zone of length 2, the interval $x \in [-1, 1]$ where D is assumed to be unitary.

[3] Hence the denomination implicit gradient model.

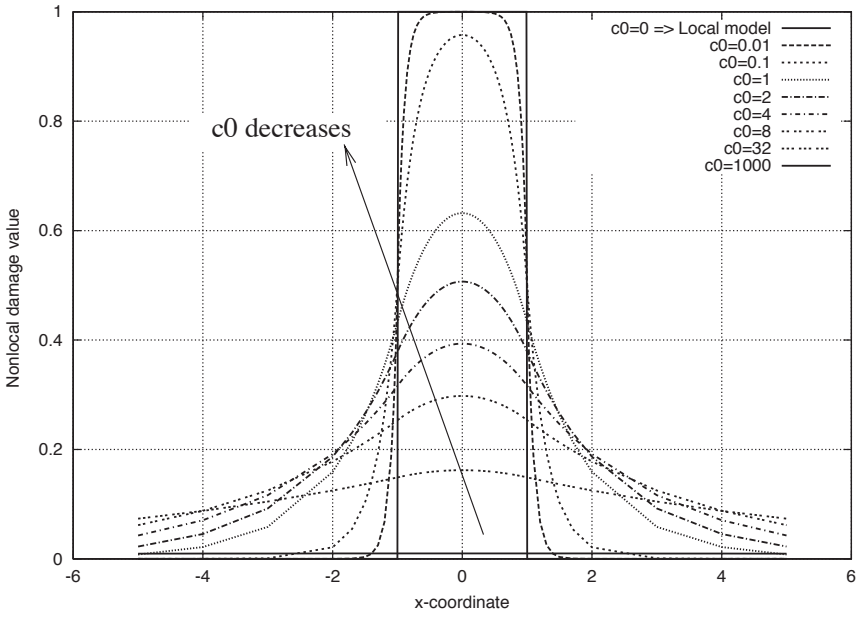

Fig. 2. The analytical solution for $\bar{D}$, as a function the x-coordinate.

The analytical solution for this case, assuming that $\lim_{x\to\infty}\bar{D}=0$ and $\lim_{x\to-\infty}\bar{D}=0$, and continuity of type C^1 everywhere, can be expressed as

$$\bar{D}=\begin{cases} -\frac{1}{2}[e^{-(1/\sqrt{c_0})}-e^{(1/\sqrt{c_0})}]e^{-(|x|/\sqrt{c_0})} & \text{for } |x|>1,\\ -\dfrac{1}{2e^{(1/\sqrt{c_0})}}[e^{(x/\sqrt{c_0})}+e^{-\left(\frac{x}{\sqrt{c_0}}\right)}]+1 & \text{for } |x|\leqslant 1. \end{cases} \tag{57}$$

The graph of $\bar{D}$ as function of x, corresponding to several values of c_0, along with the graph of D as a function of x is represented in Fig. 2.

Fig. 2 shows the effect that appears in more general situations. For a simple distribution of damage as a uniform unitary local damage distribution in the interval $x\in[-1,1]$ the gradient damage distribution is *not* uniform and is continuous. It can be thought that if a high value of the local damage variable is concentrated near a narrow zone (here the specimen has infinite length) the smoothing effect is a direct function of the c_0 value and for high values of c_0 the size of the zone where the local damage concentrates is not important for the obtained nonlocal damage distribution.

4. Numerical integration of the constitutive equations

The local damage evolution equation (39) does not have, in the general case, a closed form solution. This damage evolution equation my be rewritten, for the plastic case ($\phi=0$), under the

following form:

$$\dot{D} = G(\dot{\alpha}, D, \tilde{\boldsymbol{s}}, \tilde{p}). \tag{58}$$

This equation must be numerically integrated to be used in a finite element code. In this paper a standard unconditionally stable backward-Euler integration rule is employed. The integration is carried out in the interval $[t_n, t_{n+1}]$ where the variable t represents the pseudo-time, as in this paper the constitutive equations are assumed to be time independent. The application of the backward-Euler integration rule to (58) leads to the relation:

$$D_{n+1} - D_n - G_{n+1}(\Delta\alpha, D_{n+1}, \tilde{\boldsymbol{s}}_{n+1}, \tilde{p}_{n+1}) = 0. \tag{59}$$

This integration must be carried out to obtain the local damage both in local and the gradient approaches. The flow law (44), which is also a rate equation, can be integrated making use of a few considerations (see also Refs. [19,24]).

If there is no plastic evolution, i.e. $\dot{\boldsymbol{C}}^p = \boldsymbol{0}$, it is possible to write the following relations, making use of definition (3) of $\boldsymbol{b}^e$:

$$\boldsymbol{b}^{e,TR}_{n+1} = \boldsymbol{F}_{n+1}\boldsymbol{C}^{p-1}_n\boldsymbol{F}^{\mathrm{T}}_{n+1} = \boldsymbol{F}_{n+1}\boldsymbol{F}^{-1}_n\boldsymbol{b}^e_n\boldsymbol{F}^{-\mathrm{T}}_n\boldsymbol{F}^{\mathrm{T}}_{n+1}, \tag{60}$$

where the superscript TR indicates that (60) is an elastic trial for $\boldsymbol{b}^e_{n+1}$.

Using this elastic estimate, the elastic principal strain vector may be calculated using definition (29) for its scalar components, $\varepsilon^{TR}_i = \ln[\lambda^{TR}_i]$.

After the introduction of the so-called exponential approximation (see Refs. [24,19] for a comprehensive exposition of the von-Mises case without damage), the final elastic principal strain vector can be calculated once the variation in the plastic multiplier, $\Delta\alpha$ is known:

$$\boldsymbol{\varepsilon}_{n+1} = \boldsymbol{\varepsilon}^{TR}_{n+1} - \Delta\alpha\sqrt{\frac{3}{2}}\frac{1}{\Omega_{n+1}}\boldsymbol{v}_{n+1} \quad \text{for the local model,} \tag{61a}$$

$$\boldsymbol{\varepsilon}_{n+1} = \boldsymbol{\varepsilon}^{TR}_{n+1} - \Delta\alpha\sqrt{\frac{3}{2}}\frac{1}{\bar{\Omega}_{n+1}}\boldsymbol{v}_{n+1} \quad \text{for the gradient model.} \tag{61b}$$

The term $\boldsymbol{v}_{n+1}$ in (61) represents the flow vector (see Eq. (43)),

$$\boldsymbol{v}_{n+1} = \frac{\boldsymbol{s}_{n+1}}{\|\boldsymbol{s}_{n+1}\|} = \frac{\tilde{\boldsymbol{s}}_{n+1}}{\|\tilde{\boldsymbol{s}}_{n+1}\|}. \tag{62}$$

The application of the elastic constitutive law in principal directions, (48), results in the following equations for the flow law in terms of principal deviatoric stresses:

$$\tilde{\boldsymbol{s}}_{n+1} = \tilde{\boldsymbol{s}}^{TR}_{n+1} - 2\mu\frac{\Delta\gamma}{\Omega_{n+1}}\boldsymbol{v}_{n+1} \quad \text{for the local model,} \tag{63}$$

$$\tilde{\boldsymbol{s}}_{n+1} = \tilde{\boldsymbol{s}}^{TR}_{n+1} - 2\mu\frac{\Delta\gamma}{\bar{\Omega}_{n+1}}\boldsymbol{v}_{n+1} \quad \text{for the gradient model} \tag{64}$$

with $\Delta\gamma = \sqrt{3/2}\Delta\alpha$. The term $\tilde{\boldsymbol{s}}^{TR}_{n+1}$ is the trial deviatoric stress.

Using relation (61), the vector $\boldsymbol{v}_{n+1}$ can be written as

$$\boldsymbol{v}_{n+1} = \frac{\tilde{\boldsymbol{s}}^{TR}_{n+1}}{\|\tilde{\boldsymbol{s}}^{TR}_{n+1}\|} \tag{65}$$

which is the key property for the application of the so-called radial return algorithm (described for a much simplified case in Ref. [25]).

Finally, the integrated yield condition, for $\phi_{n+1} = 0$ can be presented as

$$\|\tilde{\boldsymbol{s}}^{TR}_{n+1}\| - 2\mu\frac{\Delta\gamma}{\Omega_{n+1}} - \sqrt{\frac{2}{3}}B_{n+1} = 0 \quad \text{for the local model,} \tag{66a}$$

$$\|\tilde{\boldsymbol{s}}^{TR}_{n+1}\| - 2\mu\frac{\Delta\gamma}{\bar{\Omega}_{n+1}} - \sqrt{\frac{2}{3}}B_{n+1} = 0 \quad \text{for the gradient model,} \tag{66b}$$

where $B_{n+1} = B(\alpha_{n+1})$.

Assuming that $\|\tilde{\boldsymbol{s}}^{TR}_{n+1}\| - \sqrt{\frac{2}{3}}B_{n+1} \neq 0$,[4] the term Ω_{n+1} in (66a) can be evaluated as in the following relation:

$$\Omega_{n+1} = \frac{2\mu\Delta\gamma}{\|\tilde{\boldsymbol{s}}^{TR}_{n+1}\| - \sqrt{\frac{2}{3}}B_{n+1}} \tag{67}$$

which means that, for the local model, the current value of the damage variable $D_{n+1} = 1 - \Omega_{n+1}$ can be directly determined by the current value of the plastic multiplier increment.

Therefore, it is sufficient to solve the nonlinear equation:

$$r = 1 - \frac{2\mu\Delta\gamma}{\|\tilde{\boldsymbol{s}}^{TR}_{n+1}\| - \sqrt{\frac{2}{3}}B_{n+1}} - D_n - G_{n+1} = 0 \tag{68a}$$

for the local model, or

$$r = 1 - \frac{2\mu\Delta\gamma}{\|\tilde{\boldsymbol{s}}^{TR}_{n+1}\| - \sqrt{\frac{2}{3}}B_{n+1}} - \bar{D}_{n+1} = 0 \tag{68b}$$

for the gradient model.

The only unknown in problem (68) is the plastic multiplier increment, $\Delta\alpha$, or alternatively $\Delta\gamma$.

It is important to note that, for the gradient model, after $\Delta\gamma$ is known through the solution of Eq. (66b), the local damage, D_{n+1} can be determined by solving Eq. (59) for D_{n+1}.

The Newton method with line-search is used to solve (66a). To apply the Newton method to this equation, the derivative of r (presented in Eqs. 68) is needed:

$$\frac{\partial r}{\partial\Delta\gamma} = \left(1 - \frac{\partial G_{n+1}}{\partial D_{n+1}}\right)\frac{\partial D_{n+1}}{\partial\Delta\gamma} - \frac{\partial G_{n+1}}{\partial\Delta\gamma} \tag{69a}$$

[4] This condition is always verified in the current implementation, because if the yield condition is satisfied with the trial deviatoric stress, there is no need for plastic multiplier correction, and hence for variation in the local damage value.

Table 2
Algorithm for the calculation of $\Delta\gamma$

$$\frac{\partial r}{\partial \Delta\gamma}\delta\Delta\gamma^* = -r$$
$$\delta\Delta\gamma = p\delta\Delta\gamma^*$$
$$\Delta\gamma = \Delta\gamma + \delta\Delta\gamma$$
$$\alpha = \alpha + \sqrt{\tfrac{2}{3}}\delta\Delta\gamma$$
$$D_{n+1} = 1 - \Omega_{n+1}(\Delta\gamma) \text{ for the local model only}$$

for the local model, and

$$\frac{\partial r}{\partial \Delta\gamma} = \frac{\partial D_{n+1}}{\partial \Delta\gamma} \tag{69b}$$

for the gradient model.

The local damage derivative in (69) can be calculated as

$$\frac{\partial D_{n+1}}{\partial \Delta\gamma} = -\frac{2\mu}{\|\tilde{\boldsymbol{s}}_{n+1}^{TR}\| - \sqrt{\tfrac{2}{3}}\,B_{n+1}} - \frac{2\mu\Delta\gamma\tfrac{2}{3}B'_{n+1}}{(\|\tilde{\boldsymbol{s}}_{n+1}^{TR}\| - \sqrt{\tfrac{2}{3}}\,B_{n+1})^2}, \tag{70}$$

where $B'_{n+1} = \partial B/\partial\alpha_{n+1}$ is the derivative of the hardening function (see (50)).

The Newton method with line-search is synthesized in Table 2.

The term p in Table 2 is the step length, obtained through a linear line-search algorithm as exposed for example in Ref. [45]. This implementation is extremely straightforward and efficient, as it avoids the solution of an equation system as required in Refs. [46,47,32].

It is important to notice that, after the value of $\Delta\gamma$ is known for the gradient model, a further step is needed to calculate the local damage variable, D_{n+1}. This is carried out solving Eq. (59) for D_{n+1}:

$$r_2 = D_{n+1} - D_n - G_{n+1} = 0 \tag{71}$$

using the Newton method.

5. Linearization and the consistent modulus

To carry out the global solution, in terms of nodal variables, through the Newton method, it is indispensable to consistently linearize the homogenized stress. The finite strain modulus is given by Eq. (32), and it is necessary to evaluate the term $\partial\tau_i/\partial\varepsilon_j$ to obtain the finite strain modulus. This term, which is denoted as $\boldsymbol{C}^{\varepsilon}$ for the local model and $\boldsymbol{C}^{\tilde{\varepsilon}}$ for the gradient model, can be referred to as the small strain consistent modulus (in principal directions). The task can be carried out taking the first variation of the homogenized stress vector,

$$\mathrm{d}\boldsymbol{\sigma}_{n+1} = \begin{Bmatrix} \mathrm{d}\tau_1 \\ \mathrm{d}\tau_2 \\ \mathrm{d}\tau_3 \end{Bmatrix} \tag{72}$$

which can be expanded as

$$\begin{aligned} \mathrm{d}\boldsymbol{\sigma}_{n+1} &= (1-D_{n+1})\,\mathrm{d}\tilde{\boldsymbol{s}}^{TR}_{n+1} - \mathrm{d}D_{n+1}(\tilde{\boldsymbol{s}}^{TR}_{n+1} + \boldsymbol{I}\,\tilde{p}_{n+1}) - 2\mu\,\mathrm{d}\Delta\gamma\boldsymbol{v}_{n+1} \\ &\quad - 2\mu\Delta\gamma\,\mathrm{d}\boldsymbol{v}_{n+1} + (1-D_{n+1})\boldsymbol{I}\,\mathrm{d}\,\tilde{p}_{n+1} \\ &= \boldsymbol{C}^{\varepsilon}_{n+1}\,\mathrm{d}\boldsymbol{\varepsilon}_{n+1} \end{aligned} \tag{73a}$$

for the local model, and

$$\begin{aligned} \mathrm{d}\boldsymbol{\sigma}_{n+1} &= (1-\bar{D}_{n+1})\,\mathrm{d}\tilde{\boldsymbol{s}}^{TR}_{n+1} - \mathrm{d}\bar{D}_{n+1}(\tilde{\boldsymbol{s}}^{TR}_{n+1} + \boldsymbol{I}\,\tilde{p}_{n+1}) - 2\mu\,\mathrm{d}\Delta\gamma\boldsymbol{v}_{n+1} \\ &\quad - 2\mu\Delta\gamma\,\mathrm{d}\boldsymbol{v}_{n+1} + (1-\bar{D}_{n+1})\boldsymbol{I}\,\mathrm{d}\,\tilde{p}_{n+1} \\ &= \boldsymbol{C}^{\bar{\varepsilon}}_{n+1}\,\mathrm{d}\boldsymbol{\varepsilon}_{n+1} + \boldsymbol{C}^{\bar{D}}\,\mathrm{d}\bar{D}_{n+1} \end{aligned} \tag{73b}$$

for the gradient model.

In order to evaluate expressions (73a), (73b), it is necessary to relate the terms $\mathrm{d}\tilde{\boldsymbol{s}}^{TR}_{n+1}$, $\mathrm{d}D_{n+1}$, $\mathrm{d}\Delta\gamma$, $\mathrm{d}\boldsymbol{v}_{n+1}$ and $\mathrm{d}\,\tilde{p}_{n+1}$ with the term $\mathrm{d}\boldsymbol{\varepsilon}_{n+1}$, and also, for the gradient model, to calculate $\boldsymbol{C}^{\bar{D}}$.

5.1. Consistent modulus for the local model

As many of the calculations required for the gradient model are common to the local model, the calculation details for the last one are described in detail.

The variation of the damage variable, $\mathrm{d}D_{n+1}$, can be related to the variation of the plastic multiplier, $\mathrm{d}\Delta\gamma$ and to the variation of the trial deviatoric stress, $\mathrm{d}\tilde{\boldsymbol{s}}^{TR}_{n+1}$, using the integrated damage evolution law (59):

$$\begin{aligned} \mathrm{d}D_{n+1} &= \frac{\sqrt{\frac{2}{3}}(\partial G/\partial\alpha_{n+1})\,\mathrm{d}\Delta\gamma + (\partial G/\partial\|\tilde{\boldsymbol{s}}^{TR}_{n+1}\|)\boldsymbol{v}_{n+1}\cdot\mathrm{d}\tilde{\boldsymbol{s}}^{TR}_{n+1} + (\partial G/\partial\,\tilde{p}_{n+1})\,\mathrm{d}\,\tilde{p}_{n+1}}{1-\partial G/\partial D_{n+1}} \\ &\Leftrightarrow \mathrm{d}D_{n+1} = a_1\,\mathrm{d}\Delta\gamma + \boldsymbol{a}_2\cdot\mathrm{d}\tilde{\boldsymbol{s}}^{TR}_{n+1} + a_3\,\mathrm{d}\,\tilde{p}_{n+1}, \end{aligned} \tag{74}$$

where

$$a_1 = \left(1-\frac{\partial G}{\partial D_{n+1}}\right)^{-1}\sqrt{\frac{2}{3}}\,\frac{\partial G}{\partial\alpha_{n+1}},$$

$$\boldsymbol{a}_2 = \left(1-\frac{\partial G}{\partial D_{n+1}}\right)^{-1}\frac{\partial G}{\partial\|\tilde{\boldsymbol{s}}^{TR}_{n+1}\|}\,\boldsymbol{v}_{n+1},$$

$$a_3 = \left(1-\frac{\partial G}{\partial D_{n+1}}\right)^{-1}\frac{\partial G}{\partial\,\tilde{p}_{n+1}}.$$

The variation of the trial deviatoric stress may be written as

$$\mathrm{d}\tilde{\boldsymbol{s}}^{TR}_{n+1} = 2\mu\,\mathrm{d}\boldsymbol{e}^{e,TR}_{n+1}, \tag{75}$$

where $\boldsymbol{e}_{n+1}^{e,TR}$ is the distortional elastic trial deformation given by

$$\boldsymbol{e}_{n+1}^{e,TR} = \boldsymbol{\varepsilon}_{n+1}^{TR} - \frac{1}{3}\boldsymbol{I}\,(\varepsilon_{1,n+1}^{TR} + \varepsilon_{2,n+1}^{TR} + \varepsilon_{3,n+1}^{TR}).$$

The variation of the effective pressure, $\tilde{p}_{n+1}$ can simply be stated as

$$\mathrm{d}\,\tilde{p}_{n+1} = \kappa \boldsymbol{I} \cdot \mathrm{d}\boldsymbol{\varepsilon}_{n+1}. \tag{76}$$

The variation of the distortional elastic trial deformation can be written as

$$\mathrm{d}\boldsymbol{e}_{n+1}^{e,TR} = \left[\boldsymbol{I}_4 - \frac{1}{3}\,\boldsymbol{I}\otimes\boldsymbol{I}\right] \cdot \mathrm{d}\boldsymbol{\varepsilon}_{n+1}^{TR},$$

where $\boldsymbol{I}_4$ represents the fourth order identity tensor.

It is worthwhile to note that, in principal directions, $\boldsymbol{I}$ can be written as a vector:

$$\boldsymbol{I} = \left\{ \begin{array}{c} 1 \\ 1 \\ 1 \end{array} \right\} \tag{77}$$

and $\boldsymbol{I}_4$ as a matrix:

$$\boldsymbol{I}_4 = \left[\begin{array}{ccc} 1 & 0 & 0 \\ 0 & 1 & 0 \\ 0 & 0 & 1 \end{array} \right]. \tag{78}$$

Taking the variation of the integrated yield condition (66), and using the last relations and relations (74) and (75) it is possible, after some algebraic manipulations, to write the following equation:

$$\begin{aligned} \mathrm{d}\Delta\gamma &= \left(\frac{2\mu \boldsymbol{v}_{n+1} - (4\mu^2 \Delta\gamma/\Omega_{n+1}^2)\boldsymbol{a}_2 - (2\mu\Delta\gamma a_3 \kappa/\Omega_{n+1}^2)\boldsymbol{I}}{(2\mu/\Omega_{n+1}) + \frac{2}{3}\kappa' + (2\mu\Delta\gamma/\Omega_{n+1}^2)a_1} \right) \cdot \mathrm{d}\boldsymbol{\varepsilon}_{n+1}^{TR} \\ &= \boldsymbol{a}_4 \cdot \mathrm{d}\boldsymbol{\varepsilon}_{n+1}^{TR}. \end{aligned} \tag{79}$$

The first variation of the damage variable can therefore be written as

$$\mathrm{d}D_{n+1} = (a_1\boldsymbol{a}_4 + 2\mu\boldsymbol{a}_2 + a_3\kappa\boldsymbol{I}) \cdot \mathrm{d}\boldsymbol{\varepsilon}_{n+1}^{TR} = \boldsymbol{a}_5 \cdot \mathrm{d}\boldsymbol{\varepsilon}_{n+1}^{TR}. \tag{80}$$

The variation of the flow vector (unitary vector), $\mathrm{d}\boldsymbol{v}_{n+1}$, is simply written as

$$\begin{aligned} \mathrm{d}\boldsymbol{v}_{n+1} &= \frac{1}{\|\tilde{\boldsymbol{s}}_{n+1}^{TR}\|}\,[\boldsymbol{I}_4 - \boldsymbol{v}_{n+1}\otimes\boldsymbol{v}_{n+1}] \cdot \mathrm{d}\tilde{\boldsymbol{s}}_{n+1}^{TR} \\ &= \frac{2\mu}{\|\tilde{\boldsymbol{s}}_{n+1}^{TR}\|} \left(\boldsymbol{I}_4 - \frac{1}{3}\,\boldsymbol{I}\otimes\boldsymbol{I} - \boldsymbol{v}_{n+1}\otimes\boldsymbol{v}_{n+1} \right) \cdot \mathrm{d}\boldsymbol{\varepsilon}_{n+1}^{TR} \\ &= \boldsymbol{a}_6 \cdot \mathrm{d}\boldsymbol{\varepsilon}_{n+1}^{TR}. \end{aligned} \tag{81}$$

It remains to relate the variation of the trial elastic strain, $\mathrm{d}\boldsymbol{\varepsilon}^{TR}_{n+1}$, with the variation of the total strain, $\mathrm{d}\boldsymbol{\varepsilon}_{n+1}$. This can be readily carried out noting the additive elastoplastic split (in principal directions), which can be stated according to the following equality:

$$\boldsymbol{\varepsilon}_{n+1} = \boldsymbol{\varepsilon}^{TR}_{n+1} + \boldsymbol{\varepsilon}^{p}_{n}, \tag{82}$$

where $\boldsymbol{\varepsilon}^{p}_{n}$ represents the last converged plastic strain, whose variation is *null*.

Using (73a), (73b), the local small strain consistent tangent modulus in principal directions can be finally written as

$$\boldsymbol{C}^{\varepsilon} = 2\mu\Omega_{n+1}\left(\boldsymbol{I}_4 - \frac{1}{3}\boldsymbol{I}\otimes\boldsymbol{I}\right) - \tilde{\boldsymbol{s}}^{TR}_{n+1}\otimes\boldsymbol{a}_5 - 2\mu\boldsymbol{v}_{n+1}\otimes\boldsymbol{a}_4 - 2\mu\Delta\gamma\boldsymbol{a}_6 - \boldsymbol{I}\otimes\boldsymbol{a}_5\,\tilde{p}_{n+1} + \kappa\Omega_{n+1}\boldsymbol{I}\otimes\boldsymbol{I}. \tag{83}$$

The matrix represented in Eq. (83) is generally unsymmetrical, resulting in an unsymmetrical finite strain modulus. This is a consequence of the nonassociative flow law.

5.2. Consistent modulus for the gradient model

The derivation of the small strain consistent modulus for the gradient model is relatively straightforward. For the term $\boldsymbol{C}^{\bar{\varepsilon}}$, it is possible to write:

$$\boldsymbol{C}^{\bar{\varepsilon}} = \bar{\Omega}_{n+1}\left[2\mu b_1\boldsymbol{I}_4 + \left(\kappa - \frac{2}{3}\,\mu b_1\right)\boldsymbol{I}\otimes\boldsymbol{I} - 2\mu b_2\boldsymbol{v}_{n+1}\otimes\boldsymbol{v}_{n+1}\right], \tag{84}$$

where

$$b_1 = 1 - 2\,\frac{\mu\Delta\gamma}{\|\tilde{\boldsymbol{s}}^{TR}_{n+1}\|} \tag{85}$$

and

$$b_2 = b_1 - 1 + \frac{1}{1 + B'_{n+1}/3\mu}. \tag{86}$$

Finally, the term $\boldsymbol{C}^{\bar{D}}$ can be calculated as

$$\boldsymbol{C}^{\bar{D}} = -\tilde{\boldsymbol{s}}^{TR}_{n+1} + \boldsymbol{I}\,\tilde{p}_{n+1}. \tag{87}$$

Another relevant term is the one resulting from the variation of the local damage evaluated with the gradient model. This term can be written according to the following notation:

$$\boldsymbol{C}^{D} = \left(\frac{\mu(\partial G/\partial\Delta\gamma)}{\mu/\bar{\Omega} + B'/3} + 2\mu\,\frac{\partial G}{\partial\|\tilde{\boldsymbol{s}}^{TR}_{n+1}\|}\right)\boldsymbol{v}_{n+1} + \frac{\partial G}{\partial\,\tilde{p}_{n+1}}\,\kappa\boldsymbol{I} \tag{88}$$

such that $\mathrm{d}D_{n+1} = \boldsymbol{C}^{D}\cdot\mathrm{d}\boldsymbol{\varepsilon}_{n+1}$ is valid for the gradient model.

6. Finite element discretization

Due to the presence of the nonlocal field (i.e. $\bar{D}$), related to the local field through the differential equation (55), a mixed finite element formulation must be used. Certain authors [6,48] adopt a quadratic interpolation for the displacement field and a linear interpolation for the nonlocal variables. With a distinct approach, de Borst in the Ref. [4] adopted a higher order of interpolation in terms of nonlocal variables due to continuity requirements.

The finite element technology presented in this paper consists of an extension of previous works dealing with enhanced strain formulations [49,15,50]. In the present context an additional feature is needed to include the nonlocal field defined through differential Eq. (55). The formulation of a 3-dimensional hexahedric element with 8 nodes and 9 enhanced strain variables is presented, where the order of interpolation for the nonlocal variables is the same as the order of interpolation in terms of the displacement vector or the position vector.

The enhanced strain concept may be described as being an enrichment of the *discretized* deformation gradient, $\boldsymbol{F}$, through an additional term $\boldsymbol{A}$, in agreement with the following notation:

$$\boldsymbol{F} = \nabla_0 \boldsymbol{x} + \boldsymbol{A}. \tag{89}$$

In the present $3D$ implementation the term $\boldsymbol{A}$ is a function of 9 internal enhanced strain variables, whereas in $2D$ [15], the typical number of enhanced strain variables may be 2 or 4.

The equilibrium equation in the integral form, including the enhanced strain term, can be written as (see also Ref. [15]):

$$\int_{V_0} \boldsymbol{\tau} : (\nabla \delta \boldsymbol{x} + \delta \boldsymbol{a}) \, \mathrm{d}V_0 = \delta W_e, \tag{90}$$

where δW_e represents the virtual work of external forces and the symbol ∇ represents the spatial gradient, in contrast with the material gradient, which is denoted as ∇_0. Note that the integration domain is the material volume, V_0. The term $\delta \boldsymbol{a}$ in (90) is a short form for the product $\delta \boldsymbol{A} \boldsymbol{F}^{-1}$.

The integral form of the differential equation (55), with homogeneous boundary condition for $\nabla_0 \bar{D}$ in the boundary's normal (see also the Ref. [6] for an analogous approach), can be written as

$$\int_{V_0} -c_0 \nabla_0 \bar{D} \cdot \nabla_0 \delta \bar{D} \, \mathrm{d}V_0 + \int_{V_0} (D - \bar{D}) \delta \bar{D} \, \mathrm{d}V_0 = 0. \tag{91}$$

The discretization of the spatial position vector, $\boldsymbol{x}$, and its scalar components, x_i, takes the usual form (see for instance [51]):

$$\boldsymbol{x} = N_k \boldsymbol{x}_k \tag{92}$$

and

$$x_i = N_k x_{ki}, \tag{93}$$

where the terms N_k represent the standard shape functions for the 8-noded hexahedric element and x_{ki} are the nodal spatial position variables.

The scalar components of the gradient $\nabla\delta\boldsymbol{x}$ are calculated resorting to the nodal spatial position variations, δx_{ki}:

$$\nabla\delta x_{ij} = N_{kj}\delta x_{ki} \tag{94}$$

with $N_{kj} = \partial N_k/\partial x_j$.

The term $\boldsymbol{A}$ in Eq. (89) is discretized according to the following relation for its scalar components:

$$A_{ij} = M_{0kj}\alpha_{ki}, \tag{95}$$

where α_{ki} with $i,k = 1,2,3$ are the internal enhanced strain variables.

The functional form of the term M_{0kj}, introduced in Eq. (95), is defined according to

$$M_{0kj} = E_k \left(\frac{\partial \xi_k}{\partial X_j}\right)\bigg|_0 \quad \text{no summation on } k \tag{96}$$

whose terms ξ_k denote the local coordinates and the terms E_k with $k = 1,2,3$ represent the following functions:

$$\begin{aligned} E_1 &= -2\xi_1(1-\xi_2^2)(1-\xi_3^2),\\ E_2 &= -2\xi_2(1-\xi_1^2)(1-\xi_3^2),\\ E_3 &= -2\xi_3(1-\xi_1^2)(1-\xi_2^2). \end{aligned} \tag{97}$$

These functions agree with previous developments in $2D$ (see Refs. [50,15]) and allow the satisfaction of the relation $M_{0kj} = 0$ in the element's boundary.

The term $\partial\xi_k/\partial X_j$ in (96) is evaluated at the element's point identified by the coordinates $\xi_k = 0$.

Using these last definitions, the scalar components of the term $\delta\boldsymbol{a}$ in (90) can therefore be evaluated as

$$\delta a_{ij} = M_{kj}\delta\alpha_{ki}, \tag{98}$$

where $M_{kj} = M_{0kl}F_{lj}^{-1}$.

The nonlocal damage is discretized using the same shape functions of the position vector in relation (92):

$$\bar{D} = N_k\bar{D}_k \tag{99}$$

whose terms $\bar{D}_k$ are the nodal variables for the nonlocal damage.

The order of the nodal and internal variables in the hexahedric element is shown in Fig. 3.

As a consequence of discretization (99), the scalar components of the material gradient of the nonlocal damage can be calculated as

$$\nabla_0\bar{D}_i = N_{0ki}\bar{D}_k \tag{100}$$

with N_{0ki} being defined (please note the use of orthogonal coordinates for $\boldsymbol{F}$) as

$$N_{0ki} = N_{kl}F_{li}. \tag{101}$$

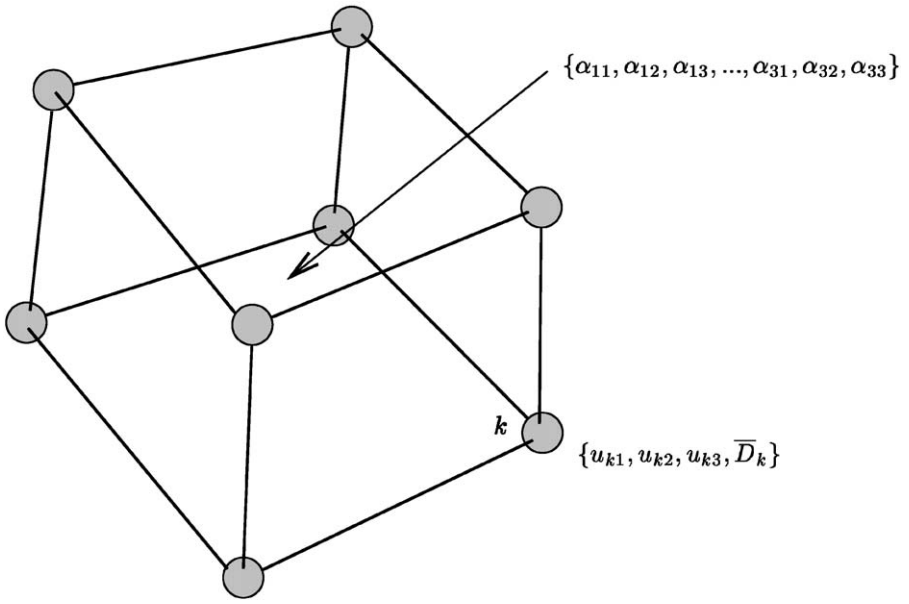

Fig. 3. Variables of the nonlocal hexahedric element.

Now the discretized equilibrium equation can be presented according to

$$\int_{V_0} \tau_{ij}(N_{kj}\delta x_{ki} + M_{kj}\delta\alpha_{ki})\,\mathrm{d}V_0 = \delta W_e \tag{102}$$

and the discretized nonlocal damage equation can be written as

$$\int_{V_0} (-c_0 N_{0li}\bar{D}_l N_{0ki}\delta\bar{D}_k + DN_k\delta\bar{D}_k - N_l N_k\bar{D}_l\delta\bar{D}_k)\,\mathrm{d}V_0 = 0. \tag{103}$$

These Eqs. (102) and (103) can be used in a straightforward manner to calculate the internal force vectors:

$$f^x_{ki} = \int_{V_0} N_{kj}\tau_{ji}\,\mathrm{d}V_0, \quad k = 1,\ldots,8, \tag{104a}$$

$$f^\alpha_{ki} = \int_{V_0} M_{kj}\tau_{ji}\,\mathrm{d}V_0, \quad k = 1,\ldots,3, \tag{104b}$$

$$f^{\bar{D}}_k = \int_{V_0} (-c_0 N_{0li}N_{0ki}\bar{D}_l + DN_k - N_l N_k\bar{D}_l)\,\mathrm{d}V_0, \quad k = 1,\ldots,8, \tag{104c}$$

where the superscripts indicate the assembling variable.

Both the internal forces in Eqs. (104a) and (104c) span the same nodes but the last one only affects the 4th nodal degree of freedom, as shown in Fig. 3 whereas the internal force in (104b) affects the first 3 nodal degrees of freedom.

Finally, with the purpose of calculating the stiffness matrix, the first variation of Eqs. (102) and (103) relative to the variables x_{ki}, α_{ki} and $\bar{D}_k$ results in the following set of terms for each element's stiffness matrix:

$$K^{xx}_{knlm} = \int_{V_0} (\delta_{nm}\tau_{ij}N_{ki}N_{lj} + N_{ki}N_{lj}C_{Tnimj})\,\mathrm{d}V_0, \tag{105a}$$

$$K^{x\alpha}_{knlm} = \int_{V_0} (\delta_{nm}\tau_{ij}N_{ki}M_{lj} + N_{ki}M_{lj}C_{Tnimj})\,\mathrm{d}V_0, \tag{105b}$$

$$K^{\alpha x}_{knlm} = \int_{V_0} (\delta_{nm}\tau_{ij}M_{ki}N_{lj} + M_{ki}N_{lj}C_{Tnimj})\,\mathrm{d}V_0, \tag{105c}$$

$$K^{\alpha\alpha}_{knlm} = \int_{V_0} (\delta_{nm}\tau_{ij}M_{ki}M_{lj} + M_{ki}M_{lj}C_{Tnimj})\,\mathrm{d}V_0, \tag{105d}$$

$$K^{x\bar{D}}_{knl} = \int_{V_0} N_l N_{kj} C^{\bar{D}}_{nj}\,\mathrm{d}V_0, \tag{105e}$$

$$K^{\alpha\bar{D}}_{knl} = \int_{V_0} N_l M_{kj} C^{\bar{D}}_{nj}\,\mathrm{d}V_0, \tag{105f}$$

$$K^{\bar{D}\bar{D}}_{kl} = -\int_{V_0} (c_0 N_{0ki}N_{0li} + N_k N_l)\,\mathrm{d}V_0, \tag{105g}$$

$$K^{\bar{D}x}_{lkn} = \int_{V_0} N_l N_{kj} C^{\bar{D}}_{nj}\,\mathrm{d}V_0, \tag{105h}$$

$$K^{\bar{D}\alpha}_{lkn} = \int_{V_0} N_l M_{kj} C^{\bar{D}}_{nj}\,\mathrm{d}V_0. \tag{105i}$$

It is important to note that the finite element stiffness matrix emerging from (105) is unsymmetrical and therefore an unsymmetrical equation solver must be used. This is not a consequence of the gradient model, but rather a consequence of the adopted nonassociative flow law, where the dissipation potential is decomposed according to Eq. (26).

It is noticeable that the terms in (105) are written in the *original* 6-dimensional stress space, and therefore a transformation is used from the principal space to the original 6-dimensional space.

The numerical implementation of the internal force vector (104) and the stiffness matrix (105), using the previous notation, is relatively straightforward.

7. Numerical examples

Two purposes are aimed with the following examples: illustrating the accuracy of the finite element formulation in solving some known problems and showing that the proposed gradient approach is effective in attenuating or removing the mesh dependency in problems involving strain softening.

7.1. A uniaxial test with central imperfection

This test consists on the stretching of a 3*D* square bar with a central material imperfection. The purpose of this test is to inspect, in a simple geometry, the capability of removing the mesh dependency without geometry complexities. The test is inspired in the ones carried out in Refs. [52,40] in which a similar test was carried out in a different constitutive context. In Ref. [40] a small strain elastic brittle behavior setting was analysed and in Ref. [52] a small strain elasto-plastic behavior was analysed but with a distinct damage model. Another recent reference with the same test but with a different damage evolution model is [41]. Here a 3*D* variant is tested. The geometry and boundary conditions are presented in Fig. 4. The presence of the imperfection forces a nonhomogeneous damage field which, if a local model is adopted, is cause of mesh-dependent response.

The material properties relative to this test are presented in Table 3, where consistent units are adopted.

The gradient model has some lower values for the energy strength of damage due to the fact that the same softening behavior is aimed. The properties related to the gradient model, c_0 and the softening measure, S_0 should be calibrated *simultaneously* for problems where the damage field is not uniform.

The tested meshes contain 22, 44, 66 and 88 elements and within each mesh, each element has exactly the same dimensions.

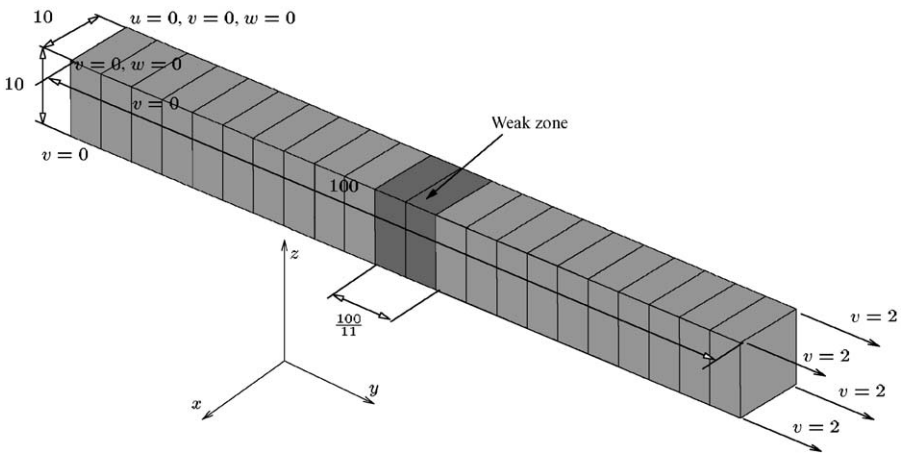

Fig. 4. The geometry and boundary conditions for the uniaxial test with central imperfection.

Table 3
The material properties for the uniaxial test with central imperfection

Property	Symbol	Value
Bulk modulus	κ	166 666.7
Shear modulus	μ	76 923.07
Yield stress	σ_Y	400
Yield stress-weak zone	σ_{YE}	360
Energy strength of damage (local model)	S_0	0.4
Energy strength of damage (local model, weak zone)	S_{0E}	0.38
Energy strength of damage (gradient model)	S_{0G}	0.2
Energy strength of damage (gradient model, weak zone)	S_{0EG}	0.18
Square of the characteristic length	c_0	80
Critical damage	D_c	0.8

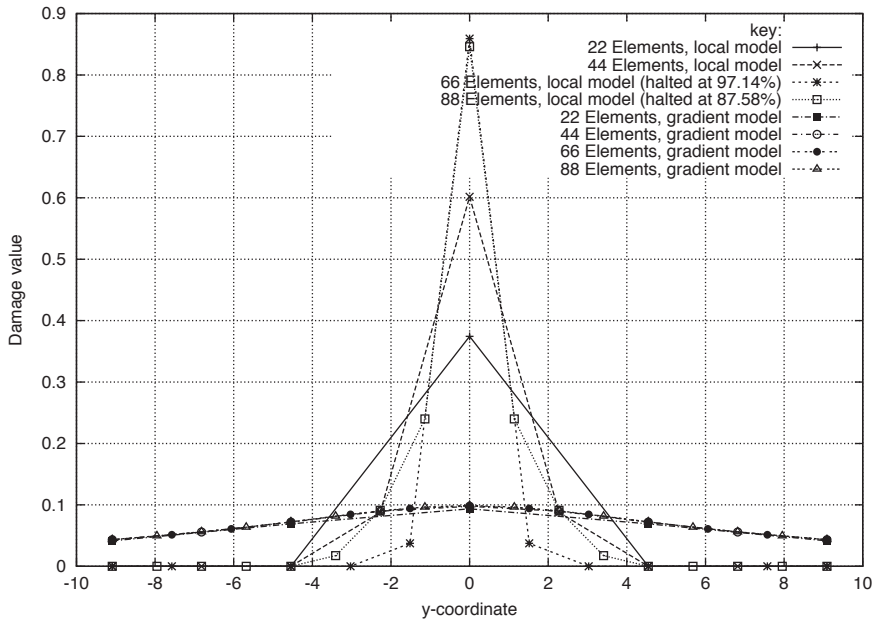

Fig. 5. The longitudinal damage distribution near the weak zone (represented in Fig. 4).

The longitudinal distribution of the damage variable near the weak zone can be observed in Fig. 5.

From the inspection of Fig. 5, it is clear that the local model presents a very mesh-dependent damage distribution along the y-axis (at least in the weak zone) and that the gradient model eliminates that dependency. A peculiar aspect to note is that there is a near-coincidence of the damage distribution curves (only at the central part of the weak zone) for the meshes containing 66 and 88 elements, however, these curves are related to different analysis phases (see Fig. 5).

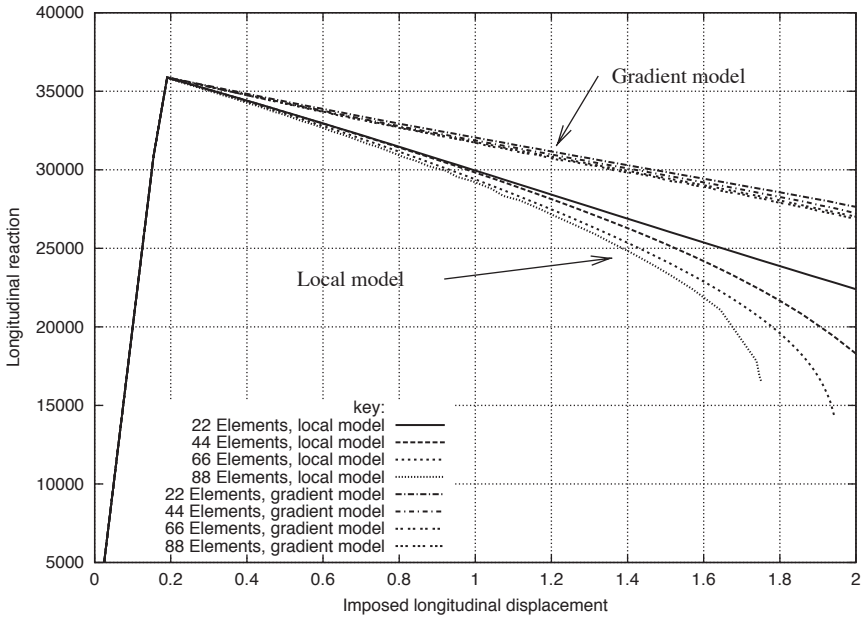

Fig. 6. The reaction curves related to the various meshes, for the local and gradient models.

In terms of reaction curves, the Fig. 6 shows a common behavior (see also Refs. [52,40]). The reaction values obtained when the local model is used are mesh dependent, and the results obtained with the gradient model are almost mesh independent.

The influence of the material parameter S_0, for a 44-element mesh using the gradient model, in the damage distribution near the weak zone, is presented in Fig. 7.

The influence of the same material parameter in the reaction curves, is shown in Fig. 8. The bumpy behavior of the reaction curves is due to the sudden evolution from D_c to D_u in the *local* damage evolution law (see Fig. 1), which is attained earlier as S_0 decreases.

In terms of influence of the parameter c_0 which controls the spreading of the damage variable near the weak zone, the damage distribution and the reaction curves are presented in Figs. 9 and 10, respectively. Clearly, the influence of the parameter c_0 is very important in terms of damage distribution and relatively unimportant in terms of reaction curves (for the values of S_0 given in Table 3).

The effect of smoothing of the damage field is visible in Fig. 9 where for higher values of c_0 the weak zone presents lower damage values and its immediate neighborhood presents higher values of the damage variable.

The determination of the area scale parameter, c_0 introduced in Eq. (55) can be carried out by measuring the relative displacement of the points inside the weak zone. The center of the bar presents a longitudinal displacement of 1. However, the planes that separate the weak zone from the rest of the bar have a relative displacement which is dependent on c_0 and S_0. The value of the material property S_0 can be determined testing a homogeneous bar, so that the damage field is uniform (and hence the gradient model is equivalent to the local model).

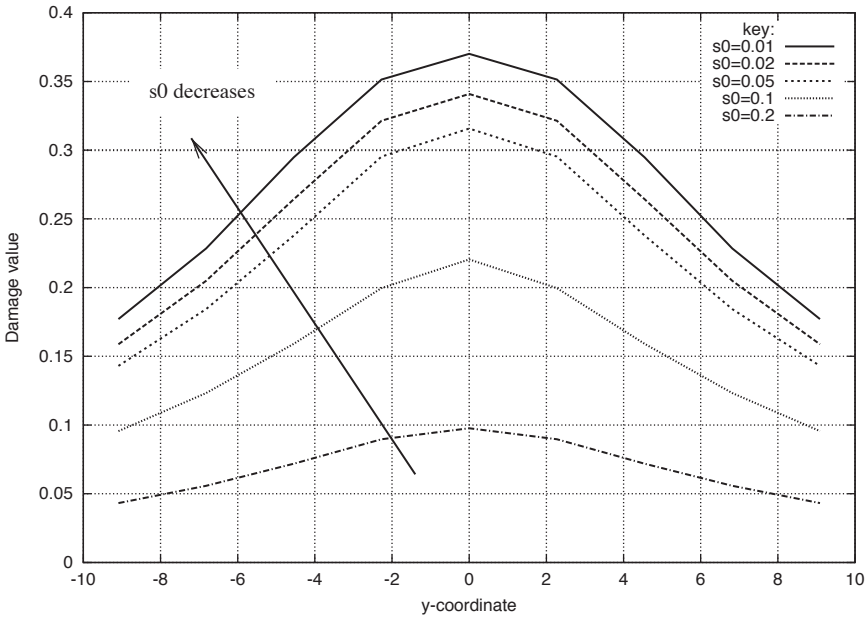

Fig. 7. The influence of the parameter S_0 in the damage distribution near the weak zone.

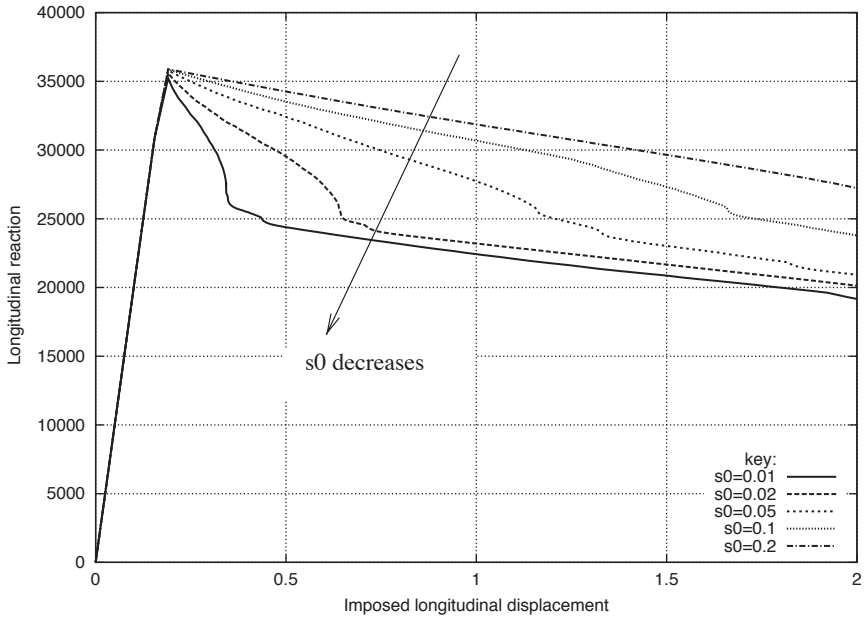

Fig. 8. The influence of the parameter S_0 in the reaction curves obtained.

As soon as the value of S_0 is known through the use of a uniform specimen, a specimen with a weak zone is tested and the relative displacement of the planes that separate the weak zone from the rest of the specimen is measured. This specimen with the weak zone can be reproduced experimentally by the introduction of a thinner cross section in the center.

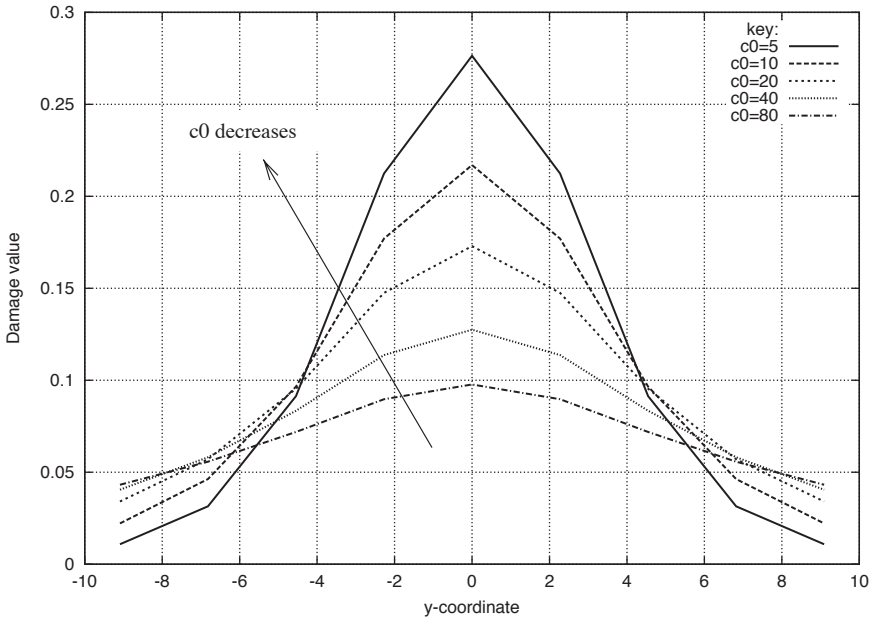

Fig. 9. The influence of the parameter c_0 in the damage distribution near the weak zone.

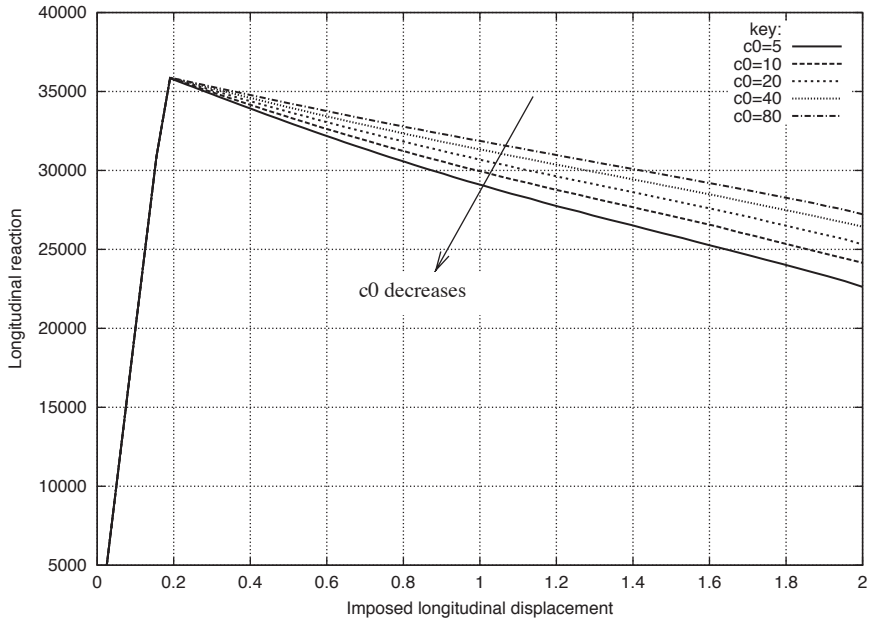

Fig. 10. The influence of the parameter c_0 in the reaction curves obtained.

The present example provides an opportunity to exploit this procedure. Fig. 11 represents, for two mesh densities (44 and 88 elements) the evolution of the described relative displacement with c_0 for a given value of $S_0 = 0.2$ in the nonweak zone.

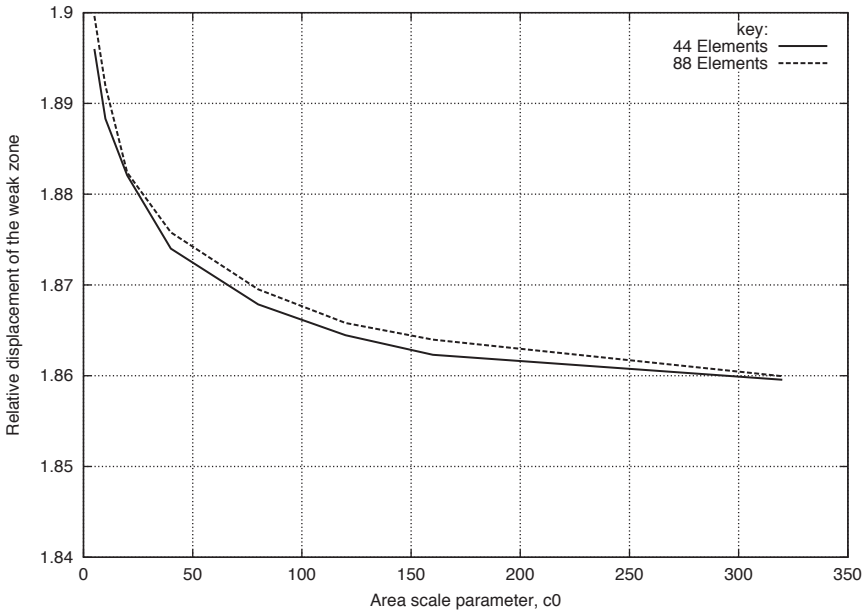

Fig. 11. The relation between the relative displacement of the weak zone and the value of c_0.

7.2. Cylindrical shell composed of two materials

This example was proposed in Ref. [53] where the Rousselier damage constitutive law was used (see also Ref. [54]). In that reference, this analysis was carried out using a shell finite element technology and a local model was adopted.

The problem consists of a cylindrical shell with a "geometry intersection" [53] and made of two distinct materials. The shell is loaded by the introduction of a line of imposed displacements. The actual geometry and dimensions can be consulted in the above reference. The mesh and boundary conditions can be viewed in Fig. 12 where the two distinct materials are painted in different colors. Only one-eighth of the actual geometry is meshed, due to existence of 3 planes of symmetry.

The material properties are exposed in Table 4 where consistent units are adopted. The represented mesh contains 864 3D elements, corresponding to the two layer shell mesh presented in Ref. [53]. Another mesh, containing 1296 3D elements is also tested, with the goal of inspecting the mesh size dependency. The deformed mesh for the sparse case is presented in Fig. 13. The damage contour plot for the sparse case and containing, for ease of visualization, only the interval $[0.05, 0.1421]$ is represented in Fig. 14.

One important aspect of the proposed analysis is that the material 1 is treated with the local model and the material 2 is treated with the gradient model. This choice is made because the damage concentrates in two main areas which are both composed of material 2.

The reaction forces obtained for the proposed mixed (local-gradient) analysis, for a completely local analysis and for the undamaged case, are presented in Fig. 15 and compared with the results obtained in Ref. [53].

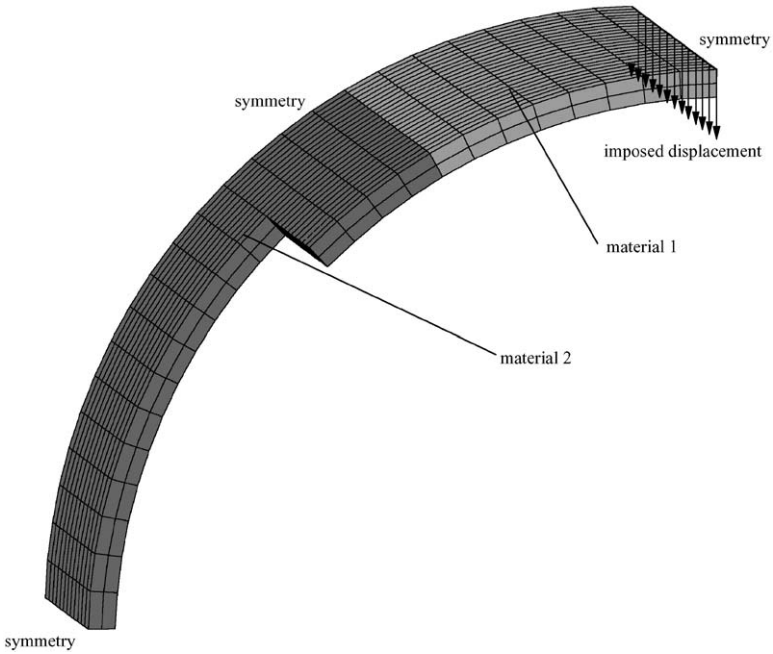

Fig. 12. The sparse mesh and boundary conditions for the cylindrical shell composed of two materials.

Table 4
The material properties for the problem represented in Fig. 12

Property	Symbol	Material 1 local	Material 2 local	Material 2 grad.
Bulk modulus	κ	175	175	175
Shear modulus	μ	80.77	80.77	80.77
Hardening law	B	$0.8 + 3.5\alpha$	$0.2 + 0.1\alpha$	$0.2 + 0.1\alpha$
Energy strength of damage	S_0	2×10^{-3}	1×10^{-4}	1×10^{-4}
Square of the characteristic length	c_0	*	*	0.6
Critical damage	D_c	0.8	0.8	0.8

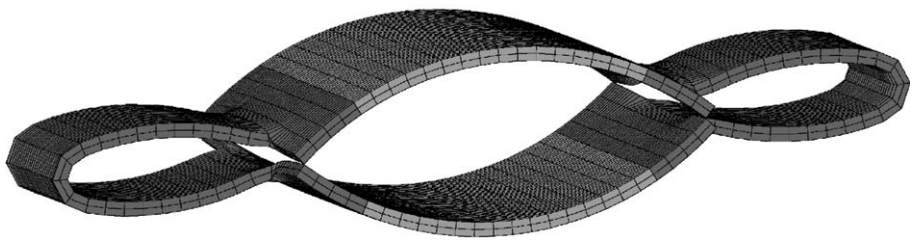

Fig. 13. Deformed mesh for the cylindrical shell composed of two materials: mixed model.

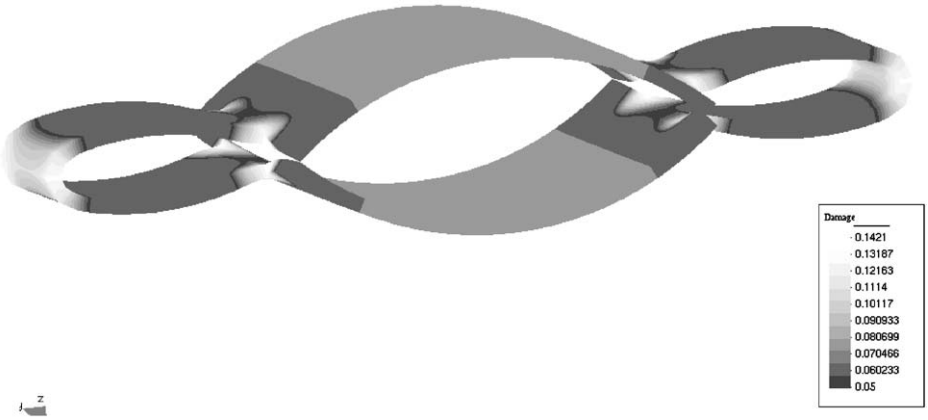

Fig. 14. Damage distribution contour plot for the cylindrical shell composed of two materials: mixed model.

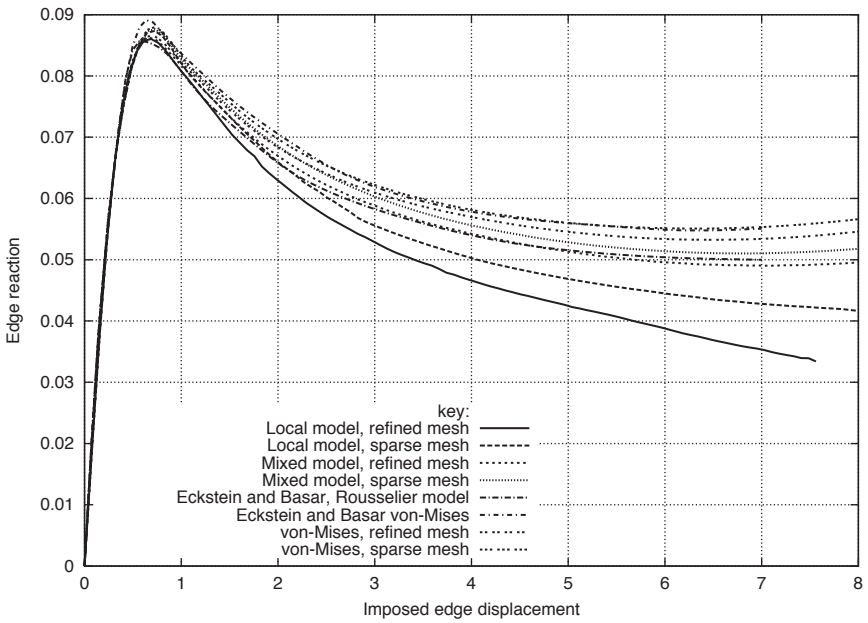

Fig. 15. Cylindrical shell: reaction forces for the proposed formulations and the results from Ref. [53].

The proposed analysis attenuates the mesh dependency that is observed if the local model is used, as it can be inspected from Fig. 15. The results obtained with the sparse mesh are very close to the ones obtained in Ref. [53] where a shell element formulation was used.

The use of the local model not only results in a much distinct behavior between the sparse and the refined mesh, but also gives rise to a premature halt in the program when the refined mesh is used (see Fig. 15). This is circumvented by the use of the mixed model.

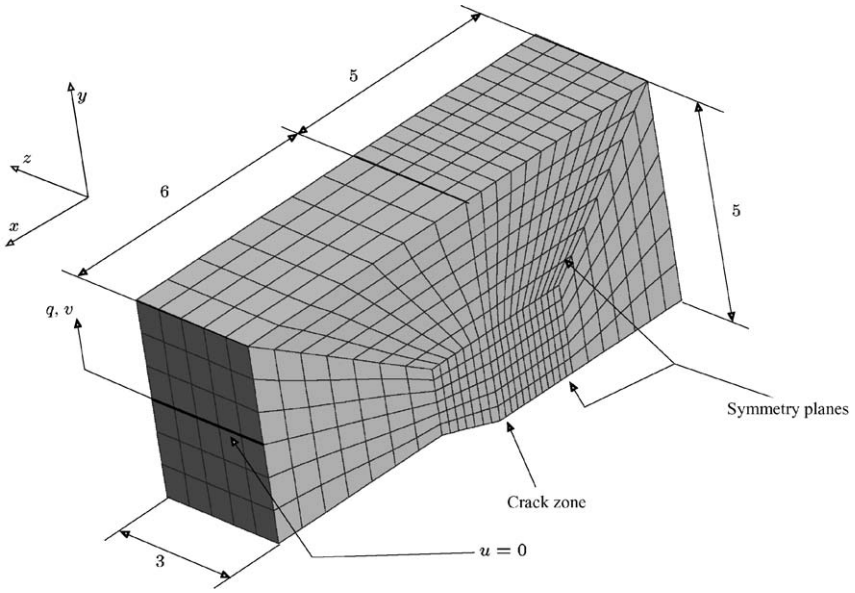

Fig. 16. Geometry and boundary conditions for the CT specimen, according to Ref. [55].

An important conclusion noticed in Ref. [53] is that, due to the damage concentration the first macroscopic crack (*macro-crack* in the notation of reference [53]) will appear in the neighborhood of the shell intersection.

For this example the mesh dependency due to strain softening is removed, as it can be seen from the reaction forces in Fig. 15.

7.3. Numerical test of a CT specimen

This test allows the inspection of the capability of the proposed model in a numerical test for which results have been published recently (see Ref. [55]). The test consists on the application of a imposed opening displacement to an idealized CT specimen. The geometry and boundary conditions for this test are presented in Fig. 16. Only one-quarter of the specimen is actually modeled, due to existence of symmetry planes. The vertical displacement, v is applied on the zone identified by $u=0$ in Fig. 16.

The adopted material properties are presented in Table 5. It is important to note that, in Ref. [55] the Rousselier damage constitutive model was adopted (see also [54]). Another difference to note is that in the present paper, a smaller value of the characteristic length, $l_0 = 0.6325$ mm instead of $l_0 = 1$ mm in Ref. [55] is used. This is because, for this value, the present model already shows mesh independence.

Two meshes are used: one containing 1655 elements and other containing 512 elements. The damage distribution over the refined deformed mesh is presented in Fig. 17, where only one-quarter of the specimen is actually represented.

Table 5
Material properties relative to the CT specimen

Property	Symbol	Value
Bulk modulus	κ	116 666.66 N/mm^2
Shear modulus	μ	87 500 N/mm^2
Hardening law	B	$1103.7(\alpha + 0.0021904)^{0.1428}$
Damage threshold	α_D	0.0
Energy strength of damage, local model	S_0	2.4 N/mm^2
Energy strength of damage, gradient model	S_{0G}	0.6 N/mm^2
Square of the characteristic length	c_0	0.4 mm^2
Critical damage	D_c	0.7

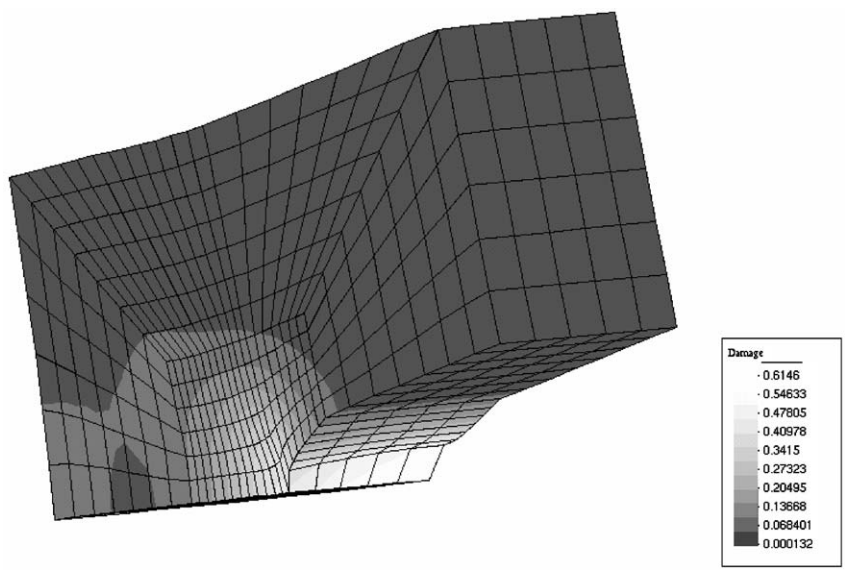

Fig. 17. Damage distribution over the deformed mesh for the gradient model and the refined mesh (only one-quarter of the model is represented and the interior crack tip is *invisible*).

The zone with the highest damage values is not the crack tip itself, but rather an interior zone at a certain distance of the crack tip. This fact has already been verified by other authors (see Ref. [56]). To observe the concerned zone, a representation of the damage variable near the interior crack tip zone is shown, with the damage interval $[0.45, 0.6146]$ in Fig. 18.

The reaction forces obtained in the line of displacement application (see Fig. 16) are presented in Fig. 19.

The reaction forces obtained with the local model are clearly mesh dependent, as can be observed in Fig. 19. The reactions obtained using the gradient model are *independent* of the mesh adopted. For comparison purposes, the reactions published in Ref. [55] are presented. It is noticeable that although the results in Ref. [55] are also mesh independent for the nonlocal model proposed in that

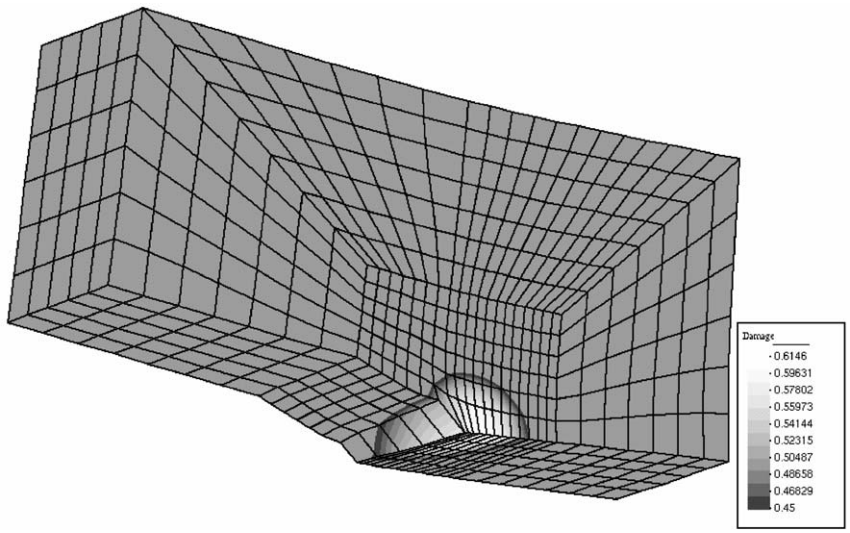

Fig. 18. Damage distribution near the interior crack tip, in the interval $[0.45, 0.6146]$.

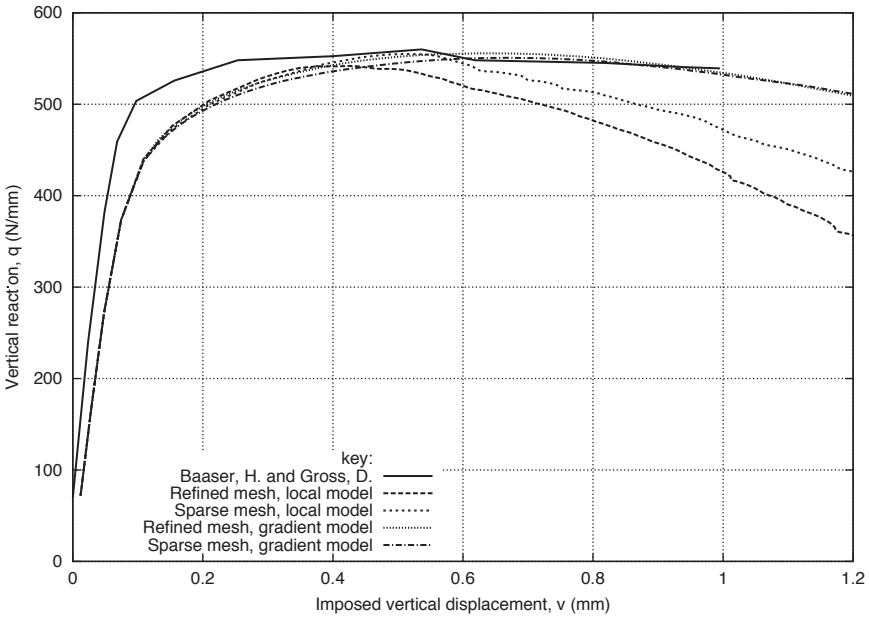

Fig. 19. Reaction forces obtained using the proposed model and the results obtained in Ref. [55].

reference, no clear softening behavior is shown, as it is visible in Fig. 19. The difference observed in Fig. 19 between the results from Ref. [55] and the ones from the present analysis in the first part of the graph can be related to the enhanced-strain formulation adopted, as a standard finite element formulation was used in Ref. [55].

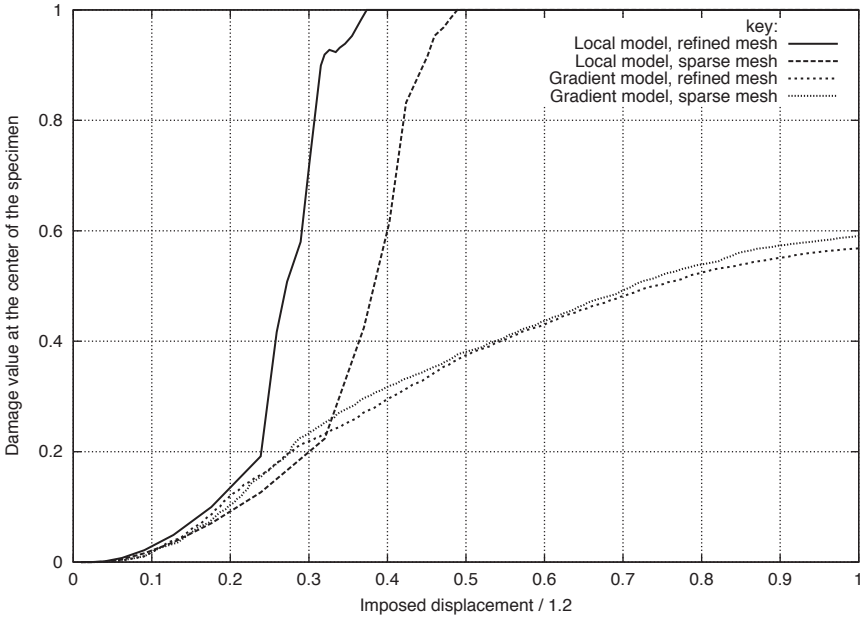

Fig. 20. Damage evolution at the center of the specimen, for two mesh densities and two damage models.

As for the damage variable at the center of the specimen, Fig. 20 shows the effect of the proposed gradient approach. Once again, the gradient model gives nearly mesh-independent results.

7.4. Stretching of a perforated plate

This example consists in the stretching of a rectangular plate which contains a central circular hole. It is documented in Ref. [57], where a local approach based on Lemaitre's damage law was adopted. The geometry and boundary conditions are presented in Fig. 21.

The material properties for this example are listed in Table 6 where consistent units are adopted.

The use of distinct values for the energy strength of damage properties is related to the difference between the two models and the need for obtaining a combination of the two properties S_0 and c_0 which actually reproduces the local model result for a given fixed mesh.

Only one-fourth of the plate is actually modeled, as symmetry conditions are exploited. A unitary thickness is used. A total displacement value of $U_2 = 6.3$ is imposed on the top part of the plate (see Fig. 21). In Ref. [57], a maximum displacement value of $U_2 = 2.65$ was imposed. Two mapped meshes are used: one with 288 elements and another one with 450 elements. The total top edge reaction is monitored and compared with the values obtained in Ref. [57] where $2D$ triangular plane stress elements were used.

The damage contour plot over the deformed mesh is represented for the gradient model using the refined mesh in Fig. 22 for an imposed displacement value of $U_2 = 2.65$. The damage initiates near the inner side of the thinner part of the plate and propagates outward, as verified in Ref. [57].

For the local model, the damage contour plot is represented in Fig. 23.

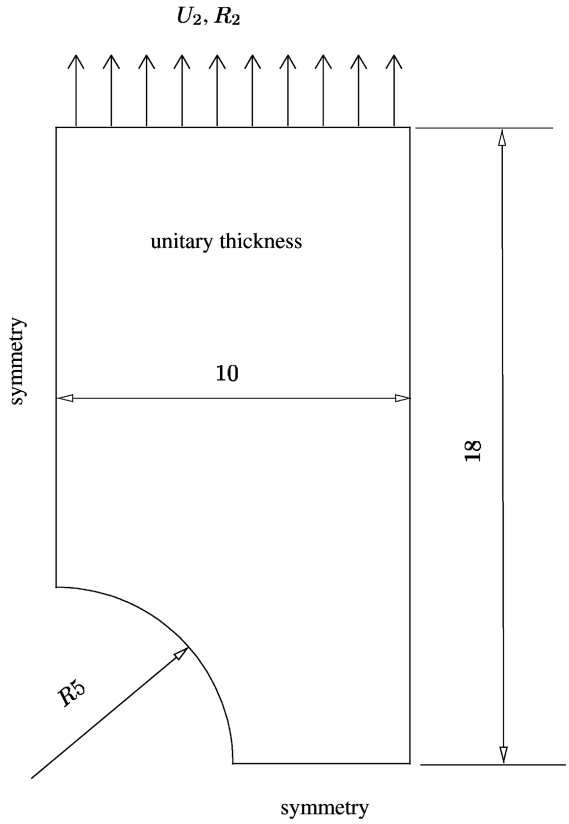

Fig. 21. The geometry and boundary conditions of the perforated plate.

Table 6
Material properties of the perforated plate

Property	Symbol	Value
Bulk modulus	κ	23.33
Shear modulus	μ	35
Hardening law	B	$0.243 + 0.2\alpha$
Damage threshold	α_D	0
Energy strength of damage, local model	S_0	4.5×10^{-3}
Energy strength of damage, gradient model	S_{0G}	3.5×10^{-3}
Square of the characteristic length	c_0	0.8
Critical damage	D_c	0.7

It is clear from the observation of the Figs. 22 and 23 that the local model presents a value close to one in the strained zone and almost all the rest of the plate is undamaged. On the contrary, the gradient model forces a spreading of the damaged zone.

In terms of reaction forces, Fig. 24 shows the results obtained with the gradient model and the local model, along with the results presented in Ref. [57].

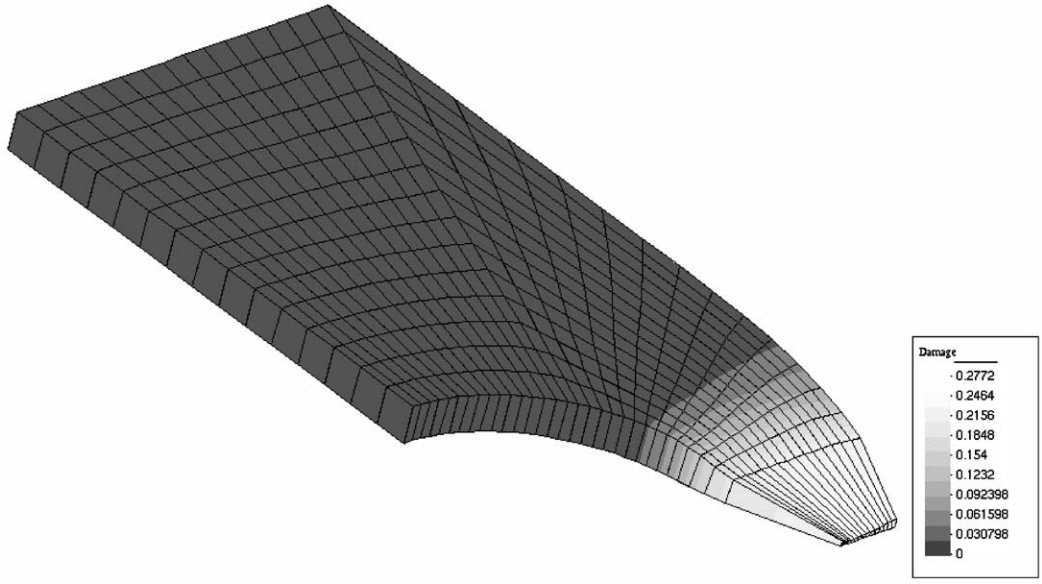

Fig. 22. The damage contour plot over the deformed mesh for the gradient model ($U_2 = 2.65$).

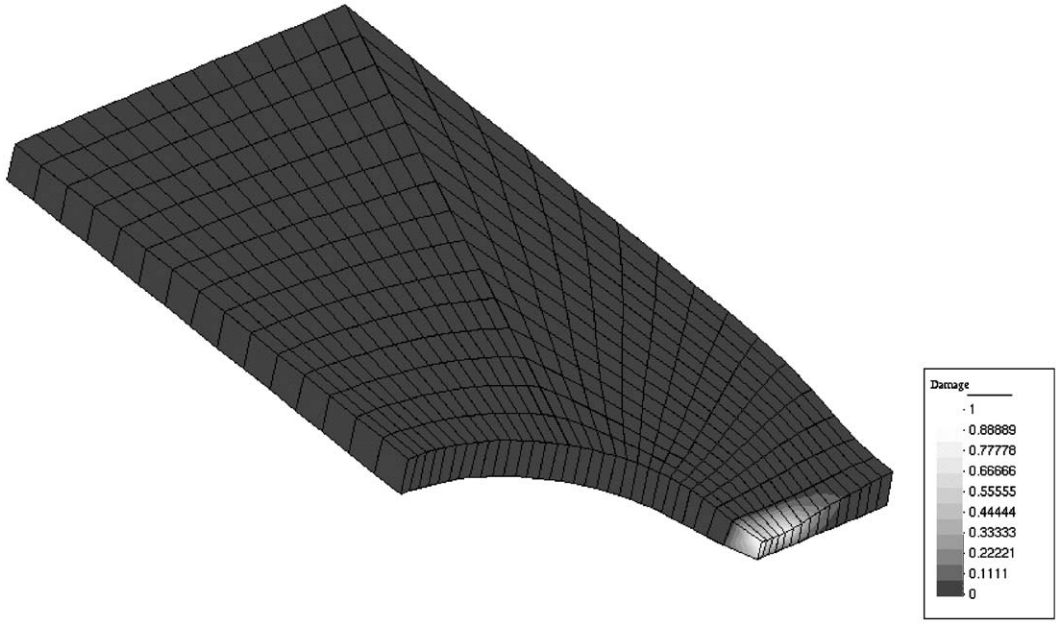

Fig. 23. The damage contour plot over the deformed mesh for the local model ($U_2 = 0.8254$).

The reaction force curves obtained using the gradient model are roughly similar to the one presented in Ref. [57]. A discussion of this problem, with some rather differently shaped curves for the reaction forces is exposed on Ref. [53].

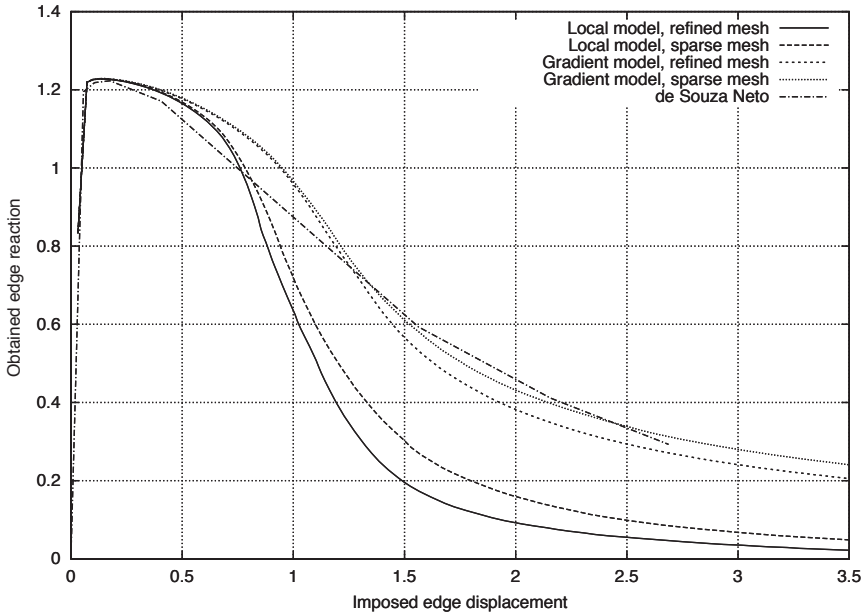

Fig. 24. Reaction forces for the perforated plate.

Table 7
Material properties for the circular bar specimen adopted in the tension test

Property	Symbol	Value
Bulk modulus	κ	164.21
Shear modulus	μ	80.1938
Hardening law	B	$0.45 + 0.12924\alpha + 0.265(1 - e^{-16.93\alpha})$
Energy strength of damage (local)	S_0	2.4×10^{-3}
Energy strength of damage (gradient)	S_{0G}	2×10^{-3}
Damage threshold	α_D	0.44
Square of the characteristic length	c_0	0.3
Critical damage	D_c	0.7

7.5. Necking of a circular bar

This example is an extension of the simulation carried out in Ref. [24] in the context of finite strain plasticity and in Ref. [34] for the $2D$ axisymmetric situation incorporating (where a simplified version of Lemaitre's damage model was tested). It consists on a circular bar subject to a uniform longitudinal displacement (a tension test). The information which can be extracted from this test is the necking displacement and the reaction forces, as measures of softening.

The material properties for this example are presented in Table 7.

As in Ref. [24], the bar has a linearly varying radius from $R_0 = 6.413$ at the end grips to $R_{\text{sym}} = 6.297566$ at the transversal symmetry plane. This varying radius induces a geometric imperfection

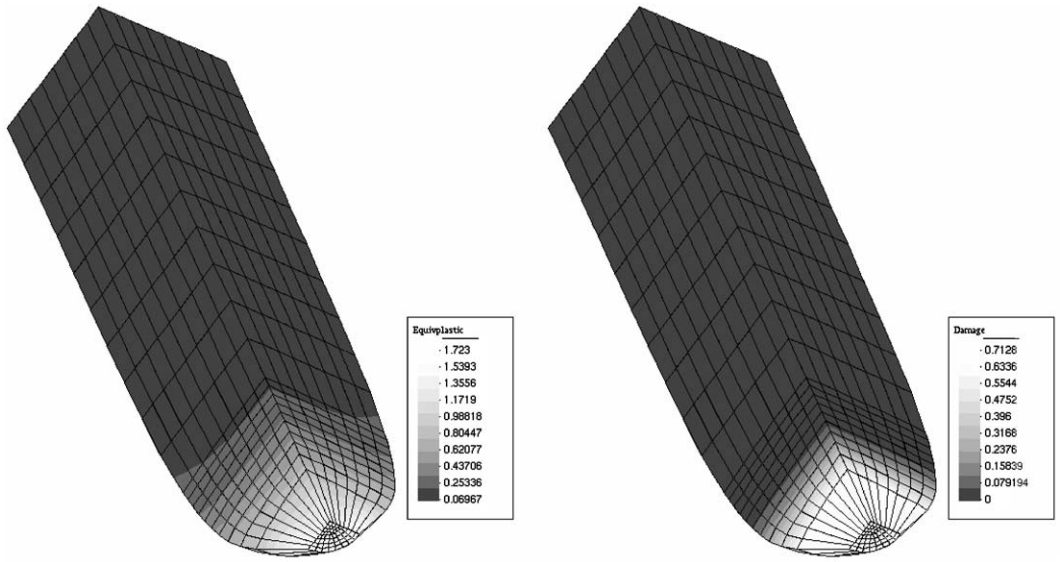

Fig. 25. Effective plastic strain and damage contour plot over the deformed mesh for an imposed longitudinal displacement of 7: gradient model, refined mesh.

and therefore necking. The total length of the specimen is $L = 53.334$. The bar is simply supported in the thinner section and is pulled in the longitudinal direction in the thicker section to a total longitudinal displacement value of 14 (7 in Refs. [24,34]). Two mesh densities are adopted: 960 elements and 378 elements.

The effective plastic strain (α) and the damage ($\bar{D}$) contour plots over the refined deformed mesh, using the gradient model are presented in Fig. 25.

The longitudinal reaction forces for the proposed gradient model and the results obtained from the $2D$ analysis carried out in Ref. [34] are presented in Fig. 26.

It is clear, from the observation of Fig. 26 that the results are almost mesh independent and that even the sparse mesh reproduces the result obtained in Ref. [34] where a $2D$ refined mesh was used.

The necking displacement (radial displacement at the transversal plane of symmetry) is presented in Fig. 27 for both the local and gradient models. It can be observed that the results are almost mesh independent for the gradient model and highly mesh dependent for the local model.

An effect of the introduction of damage in the final radial displacement at the symmetry plane is the increase of the diffuse strain localization, which constitutes necking (see Ref. [58] for a definition of diffuse strain localization and how it is a consequence primarily of *geometric* effects) due to strain softening that is not present in the undamaged case.

Therefore, in the present of damage, and hence strain softening, two effects contribute to the necking displacement: strain softening and geometric softening.

A mistake would be committed if the necking displacement is used as an indicator of the deformed volume. As damage evolves, the deformed volume should be greater than without the presence of damage. This occurs because the damage process reproduces the nucleation and growth of cavities inside the body.

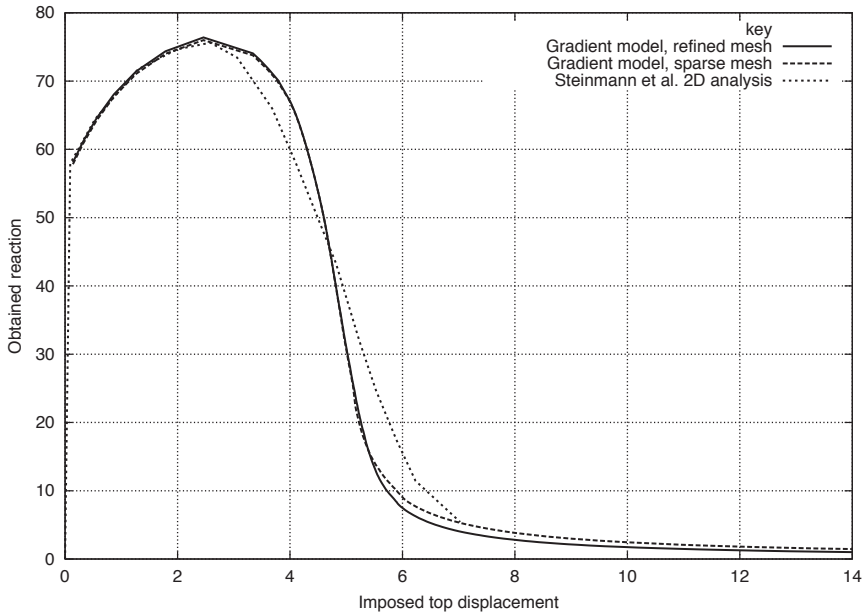

Fig. 26. Reaction forces for the gradient model, using 2 meshes and the results from Ref. [34].

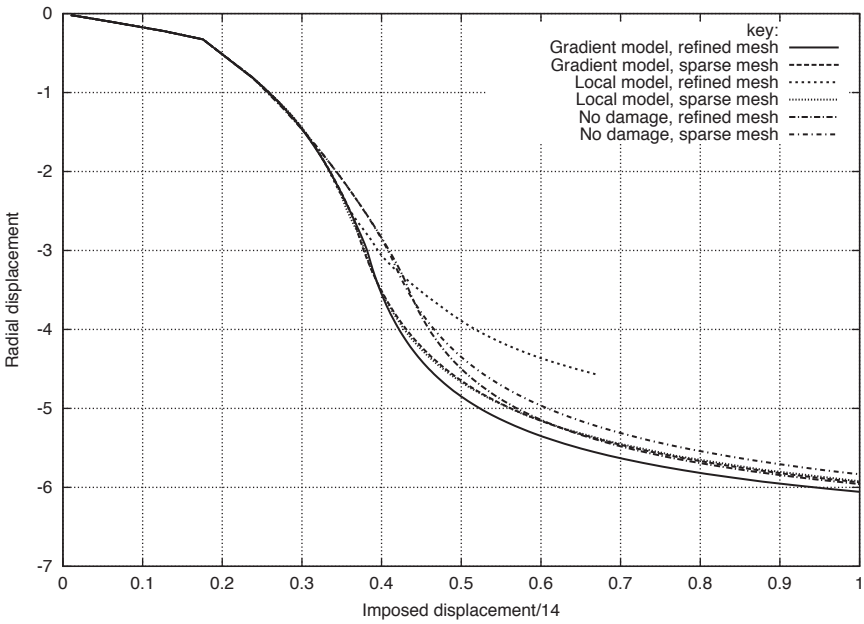

Fig. 27. Necking displacement of the specimen for various cases.

The deformed volume of 1/8 of the specimen is presented in Table 8.

From the inspection of Table 8, one may conclude that, as the imposed displacement increases, the damaged specimens have a higher volume. The fact that volume *increases* in the von-Mises

Table 8
Deformed volume of 1/8 of the specimen

Imposed displacement	0	3.5	4.2	5.6	7.0
von-Mises	840.53	841.69	841.62	841.52	843.44
Damage, local model	840.53	841.69	841.61	843.33	848.78
Damage, gradient model	840.53	841.69	841.60	841.70	845.50

model is a consequence of the increase in the elastic strain, as hardening is present (see Table 7). Therefore necking displacement is an indicator of softening (both geometric and strain softening) but not an indicator of the deformed volume.

8. Conclusions

The presented formulation, which consists on a coupled finite element technique and material model where several fields are interpolated (damage, spatial position and enhanced strain variables) is very effective in removing mesh dependency due to strain softening that affects the standard local models, usually adopted for the analysis of ductile material behavior. All the details relevant for the successful implementation of the proposed model were presented and further extensions, such as the *crack closure effect* [14] although not presented here, are easily introduced and have been already implemented within the implicit gradient approach. The present approach shows a great potential for dealing with plastic and damage anisotropy and more complex physical models, if adequate experimental evaluation of the material properties is available.

References

[1] R. de Borst, Some recent issues in computational failure mechanics, Int. J. Numer. Methods Eng. 52 (2001) 63–95.
[2] A. Simone, Assessment of a gradient-enhanced continuum damage model and its implementation, technical report tu delft report, Technical Report CM.2000.009, Koiter Institute Delft, Delft University of Technology, Faculty of Civil Engineering and Geosciences, Mechanics and Constructions Group, September 2000.
[3] R. de Borst, E. Giessen, Material Instabilities in Solids, Wiley, New York, 1998.
[4] R. de Borst, Gradient-dependent plasticity: formulation and algorithmic aspects, Int. J. Numer. Methods Eng. 35 (1992) 521–539.
[5] H. Li, N. Chandra, Analysis of crack growth and crack-tip plasticity in ductile materials using cohesive zone models, Int. J. Plast. 2002, in press.
[6] P. Steinmann, Formulation and computation of geometrically non-linear gradient damage, Int. J. Numer. Methods Eng. 46 (1999) 757–779.
[7] M.G. Geers, R.L. Ubachs, R.A. Engelen, W.A.M. Brekelmans, Large deformation gradient-enhanced hyperelasto-plasticity for ductile failure, in: European Congress on Computational Methods in Applied Sciences and Engineering, Barcelona, 11–14 September 2000, ECCOMAS.
[8] M.G.D. Geers, R.A.B. Engelen, J.M.R. Ubachs, On the numerical modelling of ductile damage with an implicit gradient-enhanced formulation, Rev. Eur. Elements Finis 10 (2001) 173–191.
[9] R.H.J. Peerlings, R. de Borst, W.A.M. Brekelmans, J.H.P. de Vree, Gradient enhanced damage for quasi-brittle materials, Int. J. Numer. Methods Eng. 39 (1996) 3391–3403.

[10] B. Nedjar, Elastoplastic-damage modelling including the gradient of damage: formulation and computational aspects, Int. J. Solids Struct. 38 (2001) 5421–5451.
[11] Z.P. Bazant, G. Pijaudier-Cabot, Nonlocal continuum damage, localization instability and convergence, J. Appl. Mech. 55 (1988) 287–293.
[12] M. Jirasek, Nonlocal models for damage and fracture: comparison of approaches, Int. J. Solids Struct. 35 (1998) 4133–4145.
[13] J. Lemaitre, Coupled elasto-plasticity and damage constitutive equations, Comput. Methods Appl. Mech. Eng. 51 (1985) 31–49.
[14] J. Lemaitre, A Course on Damage Mechanics, 2nd Edition, Springer, Berlin, 1996.
[15] J.M.A. César de Sá, P.M.A. Areias, R.M. Natal Jorge, Quadrilateral elements for the solution of elasto-plastic finite strain problems, Int. J. Numer. Methods Eng. 51 (2001) 883–917.
[16] M. Brunig, Large strain elasto-plastic theory and nonlinear finite element analysis based on metric transformation tensors, Comput. Mech. 24 (1999) 187–196.
[17] A. Ibrahimbegovic, F. Gharzeddine, Finite deformation plasticity in principal axes: from a manifold to the euclidean setting, Comput. Methods Appl. Mech. Eng. 171 (1999) 341–369.
[18] J. Lubliner, Plasticity Theory, Macmillan, New York, 1990.
[19] C. Miehe, A constitutive frame of elastoplasticity at large strains based on the notion of a plastic metric, Int. J. Solids Struct. 35 (1998) 3859–3897.
[20] C. Miehe, A formulation of finite elastoplasticity based on dual co and contravariant eigenvector triads normalized with respect to a plastic metric, Comput. Methods Appl. Mech. Eng. 159 (1998) 223–260.
[21] P. Papadopoulos, J. Lu, A general framework for the numerical solution of problems in finite elasto-plasticity, Comput. Methods Appl. Mech. Eng. 159 (1998) 1–18.
[22] J.C. Simo, A framework for finite strain elastoplasticity based on maximum plastic dissipation and the multiplicative decomposition, part i: continuum formulation, Comput. Methods Appl. Mech. Eng. 66 (1988) 199–219.
[23] J.C. Simo, A framework for finite strain elastoplasticity based on maximum plastic dissipation and the multiplicative decomposition, part ii: computational aspects, Comput. Methods Appl. Mech. Eng. 68 (1988) 1–31.
[24] J.C. Simo, Algorithms for static and dynamic multiplicative plasticity that preserve the classical return mapping schemes of the infinitesimal theory, Comput. Methods Appl. Mech. Eng. 99 (1992) 61–112.
[25] J.C. Simo, T.R. Hughes, Computational inelasticity, in: Interdisciplinary Applied Mathematics, Vol. 7, Springer, Berlin, 1998.
[26] J.C. Simo, A framework for finite strain elastoplasticity based on maximum plastic dissipation and the multiplicative decomposition, part 2: computational aspects, Comput. Methods Appl. Mech. Eng. 68 (1988) 1–31.
[27] C. Miehe, Comparison of two algorithms for the computation of fourth-order isotropic tensor functions, Comput. Struct. 66 (1998) 37–43.
[28] J. Bonet, R.D. Wood, Nonlinear Continuum Mechanics for Finite Element Analysis, Cambridge University Press, Cambridge, 1997.
[29] J.E. Marsden, J.R.H. Thomas, Mathematical Foundations of Elasticity, Dover Publications, Mineola, New York, 1993.
[30] J.C. Simo, F. Armero, Geometrically non-linear enhanced strain mixed methods and the method of incompatible modes, Int. J. Numer. Methods Eng. 33 (1992) 1413–1449.
[31] J.C. Simo, T.J.R. Hughes, Computational inelasticity, in: Interdisciplinary Applied Mathematics, Vol. 7, Springer, New York, 1998.
[32] I. Doghri, Numerical implementation and analysis of a class of metal plasticity models coupled with ductile damage, Int. J. Numer. Methods Eng. 38 (1995) 3403–3431.
[33] R. Mahnken, A comprehensive study of a multiplicative elastoplasticity model coupled to damage including parameter identification, Comput. Struct. 74 (2000) 179–200.
[34] P. Steinmann, C. Miehe, E. Stein, Comparison of different finite deformation inelasticity damage models within multiplicative elastoplasticity for ductile materials, Comput. Mech. 13 (1994) 458–474.
[35] T.L. Anderson, Fracture mechanisms in metals, in: Fracture Mechanics, Fundamentals and Applications, CRC Press, Boca Raton, FL, 1991, pp. 301–348 (Chapter 5).
[36] A.G. Atkins, Y.-W. May, Crack and craze nucleation, in: Elastic and Plastic Fracture. Metals, Polymers, Ceramics, Composites, Biological Materials, Ellis Horwood, Chichester, UK, 1985, pp. 369–430 (Chapter 5).

[37] J. Lee, G.L. Fenves, A return-mapping algorithm for plastic-damage models: 3*d* and plane stress formulation, Int. J. Numer. Methods Eng. 50 (2001) 487–506.
[38] M. Johansson, R. Mahnken, K. Runesson, Efficient integration technique for generalized viscoplasticity coupled with damage, Int. J. Numer. Methods Eng. 44 (1999) 1727–1747.
[39] R. de Borst, J. Pamin, Some novel developments in finite element procedures for gradient-dependent plasticity, Int. J. Numer. Methods Eng. 39 (1996) 2477–2505.
[40] E. Kuhl, E. Ramm, Simulation of strain localization with gradient enhanced damage models, Comput. Mater. Sci. 16 (1999) 176–185.
[41] E. Benvenuti, G. Borino, A. Tralli, A thermodynamically consistent nonlocal formulation for damaging materials, Eur. J. Mech. A/Solids, 2002, to be published.
[42] A. Zervos, P. Papanastasiou, I. Vardoulakis, A finite element displacement formulation for gradient elastoplasticity, Int. J. Numer. Methods Eng. 50 (2001) 1369–1388.
[43] J. Oliver, Continuum modelling of strong discontinuities in solid mechanics using damage models, Comput. Mech. 17 (1995) 49–61.
[44] E. Stein, P. Steinmann, C. Miehe, Instability phenomena in plasticity: modelling and computation, Comput. Mech. 17 (1995) 74–87.
[45] M.A. Crisfield, Non-Linear Finite Element Analysis of Solids and Structures, Vol. 2, Wiley, New York, 1997.
[46] E.A. de Souza Neto, D. Peric, A computational framework for a class of fully coupled models for elastoplastic damage at finite strains with reference to the linearization aspects, Comput. Methods Appl. Mech. Eng. 130 (1996) 179–193.
[47] M. Vaz Jr., D.R.J. Owen, Aspects of ductile fracture and adaptive mesh refinement in damaged elasto-plastic materials, Int. J. Numer. Methods Eng. 50 (2001) 29–54.
[48] E. Kuhl, E. Ramm, R. de Borst, An anisotropic gradient damage model for quasi-brittle materials, Comput. Methods Appl. Mech. Eng. 183 (2000) 87–103.
[49] J.M.A. César de Sá, R.M. Natal Jorge, New enhanced strain elements for incompressible problems, Int. J. Numer. Methods Eng. 44 (1999) 229–248.
[50] J.M.A. César de Sá, P.M.A. Areias, R.M. Natal Jorge, Analysis of large elasto-plastic deformation with new compatible mode elements, ECCOMAS 2000C, Book of Abstracts of the European Congress on Computational Methods in Applied Science and Engineering, Barcelona, CIMNE, Barcelona, Spain, 2000.
[51] K.-J. Bathe, Finite Element Procedures, Prentice-Hall International Editions, Englewood Cliffs, NJ, 1996.
[52] R. deBorst, J. Pamin, M.G.D. Geers, On coupled gradient-dependent plasticity and damage theories with a view to localization analysis, Euro. J. Mech. A/Solids 18 (1999) 939–962.
[53] Y. Eckstein, A. Basar, Ductile damage analysis of elasto-plastic shells at large inelastic strains, Int. J. Numer. Methods Eng. 47 (2000) 1663–1687.
[54] G. Rousselier, J.C. Devaux, G. Mottet, G. Devesa, A methodology for ductile fracture analysis based on damage mechanics: an illustration of a local approach to fracture, Nonlinear Fracture Mech. 2 (1989).
[55] H. Baaser, D. Gross, 3*d* nonlocal simulation of ductile crack growth—a numerical realization, Rev. Eur. Elements Finis 10 (2001) 353–367.
[56] H. Baaser, D. Gross, Crack analysis in ductile shells using Gurson's model, Int. J. Solids Struct. 37 (2000) 7093–7104.
[57] E.A. de Souza Neto, D. Peric, D.R.J. Owen, Continuum modelling and numerical simulation of material damage at finite strains, Arch. Comput. Methods Eng. 74 (1998).
[58] B. Dodd, Y. Bai, Ductile Fracture and Ductility With Applications to Metalworking, Academic Press, New York, 1987.